

Scalar meson photoproduction

A. Donnachie

School of Physics and Astronomy, University of Manchester, Manchester M13 9PL, England

Yu. S. Kalashnikova

ITEP, RU-117259 Moscow, Russia

(Received 16 July 2008; published 3 December 2008)

The light-quark nonstrange scalar mesons $a_0(980)$, $f_0(980)$, $f_0(1370)$, $a_0(1450)$, $f_0(1500)$, and $f_0(1710)$ are of great interest because there is no generally accepted view of their structure that can encompass $qq\bar{q}\bar{q}$, molecular, $q\bar{q}$, and glueball states in various combinations. It has been shown previously that the radiative decay of the scalar mesons to ρ and ω is a good probe of their structure and provides good discrimination among models. Scalar meson photoproduction is proposed as an alternative to measuring radiative decay, and it is shown to be a feasible proposition.

DOI: [10.1103/PhysRevC.78.064603](https://doi.org/10.1103/PhysRevC.78.064603)

PACS number(s): 25.20.Lj, 13.60.Le, 14.40.Cs

I. INTRODUCTION

The fundamental structure of light scalar mesons is still a subject of controversy. One view is that $\sigma(485)$, $\kappa(700)$, $f_0(980)$, and $a_0(980)$ are molecular or $qq\bar{q}\bar{q}$ states and thus unrelated to $q\bar{q}$ spectroscopy. Then, $a_0(1450)$ and $K_0^*(1430)$ are regarded as the $u\bar{d}$ and $u\bar{s}$ members of the same SU(3) flavor nonet of 1^3P_0 ground-state $q\bar{q}$ mesons, to which $f_0(1370)$ can be attached as the $(u\bar{u} + d\bar{d})$ member [1]. There remain two possibilities for the ninth member of the nonet: $f_0(1500)$ and $f_0(1710)$. It is frequently assumed that this surplus of isoscalar scalars in the 1300–1700 MeV mass region can be attributed to the presence of a scalar glueball [2]. This assumption is supported by calculations in quenched lattice gauge theory, which predict a scalar glueball in this mass range [3–5]. The three physical states are then viewed as mixed $q\bar{q}$ and gluonium states, although there is not agreement in detail about the mixing [6–8]. This is the first scenario we consider.

A variation of this is to consider the isoscalar, isospinor, and isovector scalars as mixed $q\bar{q}$, $qq\bar{q}\bar{q}$ states (see Refs. [9–15] and references therein). This approach is based on an effective chiral Lagrangian framework, formulated in terms of a $q\bar{q}$ and a $qq\bar{q}\bar{q}$ nonet with, in most cases, the addition of a glueball. An alternative approach, in terms of instanton dynamics, is given in Ref. [16]. Fitting to the scalar masses and some hadronic widths produces a satisfactory description of them, but no consistent picture of the mixing emerges, partly because of the different initial assumptions and partly because of the vagaries in the data. Nonetheless, the solutions with glueballs are similar to those in Refs. [6–8], particularly with respect to glueball mixing, although they do have different degrees of $q\bar{q}$ and $qq\bar{q}\bar{q}$ mixing.

Calculations in unquenched LQCD [17] suggest that the mass of the lightest glueball could be considerably lower than in the quenched case, around 1 GeV, casting doubt on this mixing model and opening up many other possible interpretations [18]. Furthermore, it has been argued that $f_0(1370)$ may not exist [18–20], although this is strongly contested

[21,22]. Should $f_0(1370)$ not exist, then the lowest scalar nonet may be taken to comprise $a_0(980)$, $f_0(980)$, $f_0(1500)$, and $K_0^*(1430)$. The $f_0(980)$ and $f_0(1500)$ are mixed such that the former is close to a singlet and the latter close to an octet. The lightest scalar glueball is a broad object extending from 400 to about 1700 MeV. This is the second scenario we consider.

Another possibility is that $\sigma(485)$, $\kappa(700)$, $f_0(980)$, and $a_0(980)$ comprise the 1^3P_0 ground-state nonet of $q\bar{q}$, although their properties are strongly influenced by coupling with a low-mass glueball [23]. In this case, in the absence of $f_0(1370)$, the $f_0(1500)$ and $f_0(1710)$ are members of the first radial 2^3P_0 scalar excitation and may also have a significant glueball component. This is the third scenario we consider.

Finally it has been suggested [22] that $f_0(1370)$ not only exists but also is a pure octet with strong coupling to $\pi\pi$, making this the dominant decay channel, in broad agreement with the results of Ref. [21]. It is further suggested that $f_0(1500)$ and $f_0(1710)$ (which are the same pole but observed on different Riemann sheets) correspond to an unmixed glueball. This is the fourth scenario we consider.

Radiative transitions offer a particularly powerful means of probing the structure of hadrons, as the coupling to the charges and spins of the constituents reveals detailed information about wave functions and can discriminate among models. If one assumes the scalar mesons to be bound $q\bar{q}^3P_0$ states, the radiative decay proceeds via a quark loop, and the corresponding matrix element can be estimated in the quark model. In such a framework, both the radiative decay of a vector meson to a scalar meson, $V \rightarrow S\gamma$ [24], and the radiative decay of a scalar meson to a vector meson, $S \rightarrow V\gamma$ [25], have been considered previously. The latter appears to be the most useful in practice. It was shown that the radiative decays of $f_0(1370)$, $f_0(1500)$, and $f_0(1710)$ are strongly affected by the degree of mixing between the basis $q\bar{q}$ states and the glueball. It is clear [25] that the discrimination among the different mixing scenarios provided by the radiative decays is strong.

The calculations of Refs. [24,25] are relevant for the first scenario we consider. They are reviewed briefly in Sec. II and then extended to calculate the radiative decays of the scalar mesons in the models appropriate to the second, third, and fourth scenarios. This calculation includes $a_0(980)$, $f_0(980)$, and $a_0(1450)$ as well as $f_0(1370)$, $f_0(1500)$, and $f_0(1710)$.

Photoproduction of the scalar mesons at medium energy provides an alternative to the direct observation of the radiative decays. It is this possibility that we explore here and show that it is viable. The dominant mechanism is Reggeized ρ and ω exchange, both of which are well understood in pion photoproduction [26]. The energy must be sufficiently high for the Regge approach to be applicable but not too high, as the cross section decreases approximately as s^{-1} . In practice, this means a photon energy of approximately 5–10 GeV, which is pertinent to experiments at the Thomas Jefferson National Accelerator Facility (JLab), both now and with the proposed upgrade. In addition to photoproduction on protons, we consider coherent photoproduction on ^4He , encouraged in this by a recently approved experiment at JLab [27]. Two advantages of coherent production are the elimination of background from baryon resonances, considerably simplifying partial-wave analysis of the mesonic final state, and the restriction to ω exchange, which is better understood in photoproduction than is ρ exchange. The photoproduction model we use is described in Sec. III with full details of the calculation in the Appendix. Results for the differential and integrated cross sections on protons and ^4He in the narrow-width approximation are also presented in that section.

Mass distributions for specific final states are obtained in Sec. IV. As it is unlikely that the charged decay modes of the scalars can be considered because of the very much larger cross sections in $\pi^+\pi^-$, K^+K^- , $2\pi^+2\pi^-$, and $\pi^+\pi^-2\pi^0$ from vector meson production, we concentrate on all-neutral channels which automatically exclude any vector meson contribution. Specifically the neutral channels are $\pi^0\pi^0$, $\eta^0\eta^0$, $\pi^0\eta^0$, and $4\pi^0$. A discussion of the branching fractions of $f_0(1370)$ is included because of the degree of ambiguity associated with this state.

There is a continuum background to the resonance production. A model for photoproduction of continuum $\pi^0\pi^0$, $\eta^0\eta^0$, and $\pi^0\eta^0$ states is presented in Sec. IV B, together with examples of the interference between these and appropriate resonances. The full details of these calculations are given in the Appendix.

Radiative transitions of scalars can also proceed via intermediate mesonic loops. Generally, the meson loop mechanism is expected to be suppressed due to large- N_C considerations. However, in some cases, the meson loop mechanism could be quite relevant, especially in connection with the $a_0(980)$ and $f_0(980)$ mesons which reside at the $K\bar{K}$ threshold, so that the admixture of the $K\bar{K}$ molecule in their wave function is expected to be large. An illustrative example of the $f_0(980)$ and $a_0(980)$ mesons photoproduced via a pseudoscalar loop mechanism is considered in Sec. V.

Our conclusions are that suitable combinations of measurements of scalar meson photoproduction can be used to clarify the status of the scalars. These are presented in Sec. VI.

II. RADIATIVE DECAYS

The most general structure of the γSV vertex is [28]

$$iF_\mu^{\gamma SV} = g_S[q_\mu(q-k) \cdot \epsilon - \epsilon_\mu q \cdot (q-k)], \quad (1)$$

where ϵ is the photon polarization vector, q and k are, respectively, the four-momenta of the photon and scalar meson, m_S is the scalar meson mass, m_V is the mass of the vector meson, and $(k-q)^2 = m_V^2$.

The radiative decay width is [28]

$$\Gamma(S \rightarrow \gamma V) = g_S^2 \frac{m_S^3}{32\pi} \left(1 - \frac{m_V^2}{m_S^2}\right)^3. \quad (2)$$

If one assumes the scalar mesons to be bound $q\bar{q}^3P_0$ states, the radiative decay proceeds via a quark loop, and the corresponding matrix element can be estimated in the quark model. The details of the radiative decay calculations we use are described in Refs. [24,25] and are summarized briefly here. Wave functions were assumed to be Gaussian, $\exp[-p^2/(2\beta_M^2)]$, multiplied by an appropriate polynomial, and β_M was a variational parameter obtained for each state from the Hamiltonian

$$H = \frac{p^2}{m_q} + \sigma r - \frac{4\alpha_s}{3} \frac{\alpha_s}{r} + C. \quad (3)$$

Standard quark-model parameters were used: $\sigma = 0.18 \text{ GeV}^2$, $\alpha_s = 0.5$, m_q is the quark mass and equal to 0.33 GeV for u and d quarks and 0.45 GeV for s quarks.

The transition amplitude for the decay at rest of meson A , mass m_A , to meson B , mass m_B , and a photon of three-momentum \mathbf{p} is

$$\mathbf{M}_{A \rightarrow B} = \mathbf{M}_{A \rightarrow B}^q + \mathbf{M}_{A \rightarrow B}^{\bar{q}}, \quad (4)$$

where $\mathbf{M}_{A \rightarrow B}^q$ and $\mathbf{M}_{A \rightarrow B}^{\bar{q}}$ describe the emission from the quark and antiquark, respectively. Explicitly, these are

$$\begin{aligned} \mathbf{M}_{A \rightarrow B}^q &= \frac{I_q}{2m_q} \int d^3k [\text{Tr}\{\phi_B^\dagger(\mathbf{k} - \frac{1}{2}\mathbf{p})\phi_A(\mathbf{k})\}(2\mathbf{k} - \mathbf{p}) \\ &\quad - i\text{Tr}\{\phi_B^\dagger(\mathbf{k} - \frac{1}{2}\mathbf{p})\sigma\phi_A(\mathbf{k})\} \times \mathbf{p}], \end{aligned} \quad (5)$$

and

$$\begin{aligned} \mathbf{M}_{A \rightarrow B}^{\bar{q}} &= \frac{I_{\bar{q}}}{2m_q} \int d^3k [\text{Tr}\{\phi_A(\mathbf{k})\phi_B^\dagger(\mathbf{k} + \frac{1}{2}\mathbf{p})\}(2\mathbf{k} + \mathbf{p}) \\ &\quad - i\text{Tr}\{\phi_A(\mathbf{k})\sigma\phi_B^\dagger(\mathbf{k} + \frac{1}{2}\mathbf{p})\} \times \mathbf{p}], \end{aligned} \quad (6)$$

where I_q and $I_{\bar{q}}$ are isospin factors.

The differential decay rate is given by

$$\frac{d\Gamma}{d\cos\theta} = p \frac{E_B}{m_A} \alpha I \sum |\mathbf{M}_{A \rightarrow B}|^2, \quad (7)$$

where the sum is over final-state polarizations, and $I = I_q^2 = I_{\bar{q}}^2$ is the isospin factor for neutral mesons.

It was shown in Refs. [24,25] that the model gives good agreement with existing data and in Ref. [25] that, in general, the uncertainty due to the use of Gaussian wave functions is less than 10%.

In Ref. [25], the radiative decays of $f_0(1370)$, $f_0(1500)$, and $f_0(1710)$ were considered assuming that they are mixed

TABLE I. Effects of mixing on the radiative decays of the scalars to ρ [25]. The radiative widths, in keV, are given for the three different mixing scenarios described in the text: light glueball (L), medium-weight glueball (M), and heavy glueball (H). The radiative decays of the scalars to ω are $\frac{1}{9}$ of these.

Decay	L	M	H
$f_0(1370) \rightarrow \gamma\rho$	443	1121	1540
$f_0(1500) \rightarrow \gamma\rho$	2519	1458	476
$f_0(1710) \rightarrow \gamma\rho$	42	94	705

states of the $(u\bar{u} + d\bar{d})$ and $s\bar{s}$ members of the ground-state 1^3P_0 nonet with a scalar glueball. Three different mixing possibilities have been proposed [6,7]: the bare glueball is lighter than the bare $n\bar{n}$ state [7]; its mass lies between the bare $n\bar{n}$ state and the bare $s\bar{s}$ state [7]; or it is heavier than the bare $s\bar{s}$ state [6]. We denote these three possibilities by L, M, and H, respectively. The results from Ref. [25] for each are given in Table I.

In principle, an important check on the reliability of these calculations and their application to photoproduction would be provided by the radiative decay of $a_0(1450)$, as this does not have the complication of glueball mixing. Again, assuming that it is a member of the ground-state scalar nonet, its decay width to $\rho\gamma$ is

$$\Gamma(a_0(1450) \rightarrow \rho\gamma) = 298 \text{ keV}, \quad (8)$$

and its decay to $\omega\gamma$ is a factor of 9 larger.

In scenario II, the $a_0(980)$, $f_0(980)$ and $f_0(1500)$ mesons together with $K_0^*(1430)$ form the ground-state nonet, with $f_0(980)$ and $f_0(1500)$ mixed such that the former is close to a singlet and the latter close to an octet. The radiative decay of $f_0(1500)$ can be calculated in the same model as before, with the result shown in Table II. For $a_0(980)$ and $f_0(980)$, we use the results of Ref. [28], also shown in Table II, with the $f_0(980)$ width corrected for the assumption that $f_0(980)$ is a singlet.

In scenario III, $a_0(1450)$ is a member of the first radial 2^3P_0 excitation, as it is in scenario II, together with $f_0(1500)$, $f_0(1710)$, and $K_0^*(1430)$. The radiative widths of $a_0(1450)$ and $f_0(1500)$ calculated on the basis of this assumption are given in Table III. This calculation is much more sensitive to the choice of parameters than is the ground-state calculation, so the results in Table III are not as reliable as those in Tables I and II.

TABLE II. Radiative widths in keV of the $a_0(980)$, $f_0(980)$, and $f_0(1500)$ mesons to ρ assuming that they are all members of the ground-state nonet, and that $f_0(980)$ and $f_0(1500)$ are mixed such that the former is a singlet and the latter is an octet. For the isoscalars the radiative widths to ω are $\frac{1}{9}$ of these, and that for $a_0(980)$ is a factor of 9 larger.

Decay	Width
$a_0(980) \rightarrow \gamma\rho$	14
$f_0(980) \rightarrow \gamma\rho$	83
$f_0(1500) \rightarrow \gamma\rho$	986

TABLE III. Radiative widths in keV of the $a_0(1450)$ and $f_0(1500)$ mesons to ρ assuming that they are members of the first radially excited nonet. The radiative widths to ω are a factor of 9 larger for the $a_0(1450)$ and $\frac{1}{9}$ for the $f_0(1500)$.

Decay	Width
$a_0(1450) \rightarrow \gamma\rho$	65
$f_0(1500) \rightarrow \gamma\rho$	679

Finally, scenario IV is analogous to scenario II with $f_0(1370)$ replacing $f_0(1500)$ as the octet member of the ground-state nonet. Its decay width to $\rho\gamma$ is

$$\Gamma(f_0(1370) \rightarrow \rho\gamma) = 757 \text{ keV}. \quad (9)$$

III. SCALAR PHOTOPRODUCTION

In this section, we develop the formalism for scalar photoproduction and present the differential and integrated cross sections in the narrow-width limit of the scalars for each of the four scenarios considered.

A. Cross section formalism

Let q , p_1 , k , p_2 be the four-momenta of, respectively, the photon, initial proton, scalar meson, and recoil proton. The γSV vertex has the form given in Eq. (1). The $SV\gamma$ coupling, g_S , is obtained from the radiative decay width [Eq. (2)] and is assumed to be constant. The VNN vertex is

$$F_v^{VNN} = ig_V\gamma_\nu - g_T\sigma_{\nu\tau}(p_2 - p_1)_\tau. \quad (10)$$

The ωNN couplings are rather well defined [29]. We have used $g_V^\omega = 15$ and $g_T^\omega = 0$, as this gives a good description of π^0 photoproduction [26]. The ρNN couplings are not so well defined, with two extremes: strong coupling [29] or weak coupling [30–32]. We are again guided by pion photoproduction [26] and choose the strong coupling solution with $g_V^\rho = 3.4$ and $g_T^\rho = 11 \text{ GeV}^{-1}$.

The vector meson propagator is

$$\begin{aligned} P_{\mu\nu}^V &= \frac{1}{m_V^2 - t} \left\{ g_{\mu\nu} - \frac{1}{m_V^2} (p_2 - p_1)_\mu (p_2 - p_1)_\nu \right\} \\ &= \frac{1}{m_V^2 - t} \left\{ g_{\mu\nu} - \frac{1}{m_V^2} (q - k)_\mu (q - k)_\nu \right\}. \end{aligned} \quad (11)$$

The complete photoproduction amplitude with the vector meson exchange mechanism is then

$$M_\mu(s, t)\epsilon_\mu = \bar{u}(p_2) (A_{\mu\nu}\gamma_\nu + B_\mu) u(p_1)\epsilon_\mu, \quad (12)$$

where

$$A_{\mu\nu} = a[g_{\mu\nu}(q \cdot k) - k_\mu q_\nu] = a[g_{\mu\nu}(q \cdot p) - p_\mu q_\nu], \quad (13)$$

with

$$a = \frac{g_S(g_V + 2m_p g_T)}{m_V^2 - t}, \quad (14)$$

and

$$\begin{aligned} B_\mu &= b[p_{1\mu}(q \cdot k) - k_\mu(q \cdot p_1)] \\ &= b[p_{1\mu}(q \cdot p) - p_\mu(q \cdot p_1)], \end{aligned} \quad (15)$$

with

$$b = -\frac{2g_s g_T}{m_V^2 - t}. \quad (16)$$

For the exchange of a single vector meson, we find (see Appendix)

$$\begin{aligned} |M(s, t)|^2 &= -\frac{1}{2}aa^*[s(t-t_1)(t-t_2) + \frac{1}{2}st(t-m_S^2)^2] \\ &\quad -\frac{1}{2}(ab^* + a^*b)m_p s(t-t_1)(t-t_2) \\ &\quad -\frac{1}{8}bb^*s(4m_p^2 - t)(t-t_1)(t-t_2), \end{aligned} \quad (17)$$

where t_1 and t_2 are the kinematical boundaries given by Eq. (A7), and the differential cross section is

$$\frac{d\sigma}{dt} = \frac{|M(s, t)|^2}{16\pi(s - m_p^2)^2}. \quad (18)$$

B. Reggeization

The standard prescription for Reggeizing the Feynman propagators in Eq. (17), assuming a linear Regge trajectory $\alpha_V(t) = \alpha_{V0} + \alpha'_V t$, is to make the replacement

$$\begin{aligned} \frac{1}{t - m_V^2} &\rightarrow \left(\frac{s}{s_0}\right)^{\alpha_V(t)-1} \frac{\pi\alpha'_V}{\sin(\pi\alpha_V(t))} \\ &\times \frac{-1 + e^{-i\pi\alpha_V(t)}}{2} \frac{1}{\Gamma(\alpha_V(t))}. \end{aligned} \quad (19)$$

This simple prescription automatically includes the zero observed at $t \approx -0.5 \text{ GeV}^2$ in both ρ and ω exchange and provides a satisfactory description of the ρ and ω exchange contributions to pion photoproduction [26]. We know that this approximation is not precise, as there are additional contributions, in particular from Regge cuts that are clearly required by finite-energy sum rules [33–35] and, for π^0 photoproduction, from the trajectory associated with $b_1(1235)$ exchange [26,34,35]. However, the overall effect of these additional contributions is small, the principal effects being to weaken the dip in the cross section and to modify the energy dependence at large $|t|$. The prescription (19) does not require the addition of form factors at either vertex when applied to pseudoscalar photoproduction, so we adopt the same procedure here. We assume nondegenerate ρ and ω trajectories

$$\begin{aligned} \alpha_\rho &= 0.55 + 0.8t, \\ \alpha_\omega &= 0.44 + 0.9t. \end{aligned} \quad (20)$$

For photoproduction on ${}^4\text{He}$ we assume that the cross section is given by

$$\frac{d\sigma(\gamma N \rightarrow f_0\text{He})}{dt} = \frac{d\sigma(\gamma N \rightarrow f_0N)}{dt} (4F_{\text{He}}(t))^2, \quad (21)$$

where $F_{\text{He}}(t)$ is the helium form factor [36]

$$F_{\text{He}}(t) \approx e^{9t}. \quad (22)$$

The justification for assumption (21) is the low level of nuclear shadowing observed on ${}^4\text{He}$ at the energies with which we are

concerned, for both pion and photon total cross sections [37]. Writing

$$\sigma_{hA} = A_{\text{eff}}\sigma_{hN}, \quad (23)$$

where h can be a pion or a photon, it is found that $A_{\text{eff}} \approx 0.9$ at the energies in which we are interested. Furthermore, the detailed behavior of A_{eff} as a function of photon energy and nucleus is rather well described by a simple vector-dominance model [37].

C. Narrow-width cross sections

1. Scenario I

The differential cross sections for photoproduction of $f_0(1370)$, $f_0(1500)$, and $f_0(1710)$ on protons and ${}^4\text{He}$ at $E_\gamma = 5 \text{ GeV}$ are shown in Fig. 1, and the integrated cross sections are given in Table IV. In each case, results are given for the three possible glueball masses: light (L), medium (M), and heavy (H). The cross sections for photoproduction on protons decrease with energy at the rate expected from Eq. (19), so at $E_\gamma = 10 \text{ GeV}$, they are about half of those in Table IV. However, the cross sections for photoproduction on ${}^4\text{He}$ do not decrease, and for $f_0(1500)$ and $f_0(1710)$ they actually increase. This is due to the combined effect of the ${}^4\text{He}$ form factor enhancing the contribution from small t and the maximum of the differential cross section on protons moving to smaller t with increasing energy. Note that for ${}^4\text{He}$, it is necessary to have $|t| \gtrsim 0.1 \text{ GeV}^2$, as this is the minimum achievable momentum transfer at which the recoiling α particle can be detected [38].

The cross sections for photoproduction on ${}^4\text{He}$ are very much smaller than those for photoproduction on protons. There are three reasons for this.

- (i) Switching off ρ exchange for photoproduction on protons reduces the cross section by a factor of about 16, canceling the factor 16 from coherent production.
- (ii) The helium form factor suppresses the cross section except at very small t .
- (iii) There is the experimental requirement that $|t| \gtrsim 0.1 \text{ GeV}^2$ for the recoiling helium to be detected.

Obviously, the cross sections for light, medium, and heavy glueball masses reflect directly the radiative decay widths of Table I; and, if it were practical, ratios of cross sections $f_0(1370) : f_0(1500) : f_0(1710)$ would give an immediate

TABLE IV. Integrated photoproduction cross sections in nanobarns on protons and ${}^4\text{He}$ at $E_\gamma = 5 \text{ GeV}$ for the three different mixing scenarios: light (L), medium-weight (M), and heavy (H) glueballs.

Scalar	Proton			${}^4\text{He}$		
	L	M	H	L	M	H
$f_0(1370)$	27.1	68.6	94.2	0.64	1.63	2.23
$f_0(1500)$	89.9	52.1	17.0	1.55	0.90	0.29
$f_0(1710)$	0.7	1.6	11.8	0.0026	0.0058	0.043

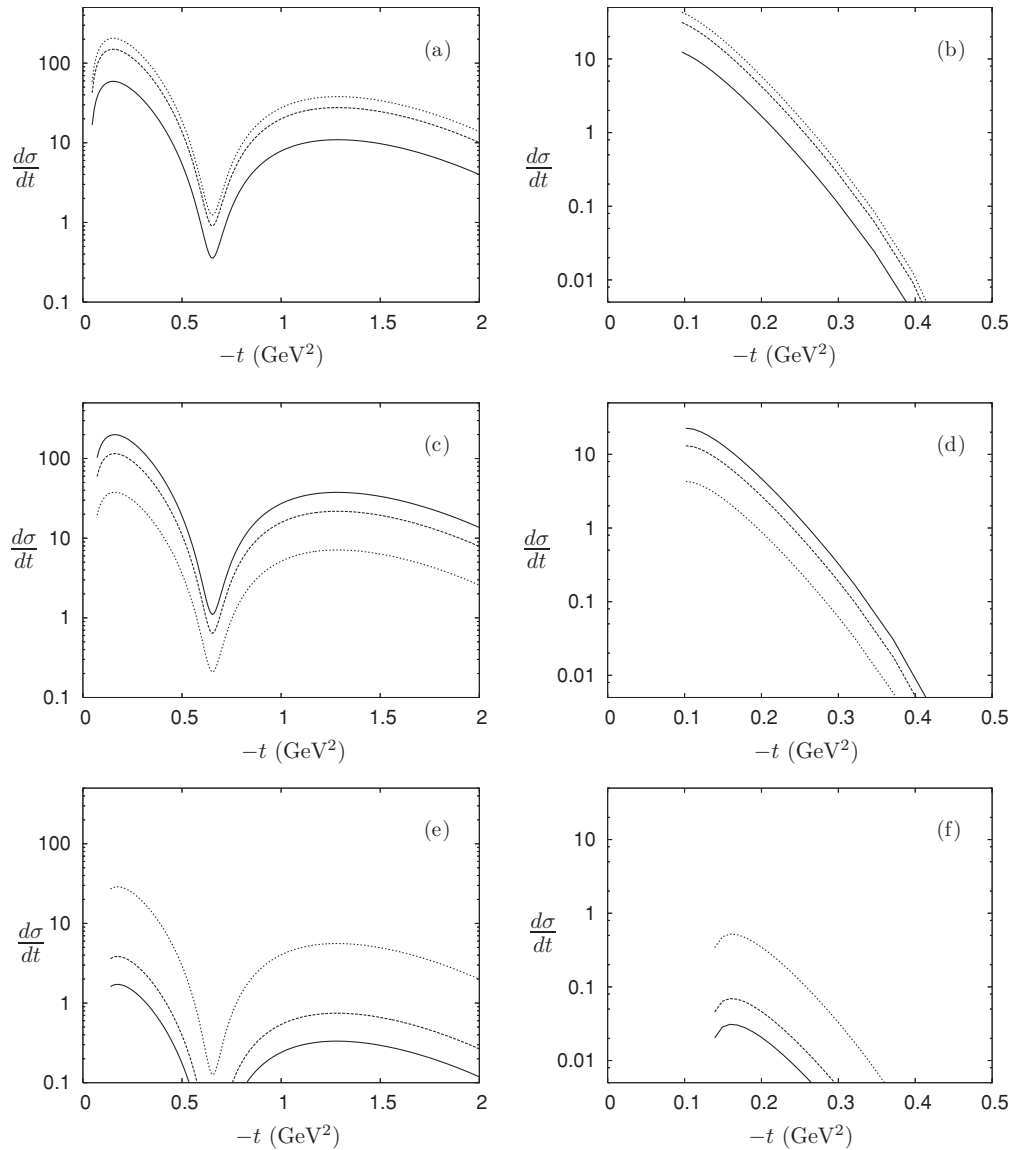


FIG. 1. Scenario I. Differential photoproduction cross sections on protons (left column) and ${}^4\text{He}$ (right column) in nb GeV^{-2} for $f_0(1370)$ (top row), $f_0(1500)$ (middle row), and $f_0(1710)$ (bottom row) at $E_\gamma = 5 \text{ GeV}$. The glueball masses are L (solid), M (dashed), and H (dotted) in each figure.

result and “weigh” the glueball. The change from L to H is more than a factor of 5, L to M nearly a factor of 2, and M to H nearly a factor of 3. Coherent production on ${}^4\text{He}$, if practical, would be particularly important quite apart from the elimination of contributions from excited baryons. Not only are the trajectories associated with ρ and $b_1(1235)$ exchange excluded, but also any Regge cut effects should be comparable for each scalar, so in the ratios the uncertainty in their contribution will be minimized. The ratios also remove any ambiguity associated with form factors and the ωNN coupling. However, as we shall see, the situation is not nearly so clear-cut when we come to consider particular final hadronic states. In particular, once the standard $\pi\pi$ branching fractions (see Table VII in Sec. IV) are taken into account, the cross sections for $f_0(1370)$, $f_0(1500)$, and $f_0(1710)$ photoproduction on ${}^4\text{He}$ in specific channels are too small to be practical. However,

$f_0(1370)$ would be an exception if the $\pi\pi$ branching fraction suggested by Bugg [21] is correct. See the discussion relating to Table VII in Sec. IV.

The integrated photoproduction cross sections for $a_0(1450)$ are 98 nb on protons and 21 nb on ${}^4\text{He}$. In contrast to the isoscalars, the cross section for photoproduction of the isovector $a_0(1450)$ on ${}^4\text{He}$ is not strongly suppressed, as its dominant radiative decay is to $\omega\gamma$. The differential cross sections for $a_0(1450)$ photoproduction on protons and ${}^4\text{He}$ are shown in Fig. 2. In this scenario, $a_0(980)$ and $f_0(980)$ are not $n\bar{n}$ states, and discussion of them is deferred until Sec. V.

2. Scenario II

In this scenario, the lowest nonet now comprises $a_0(980)$, $f_0(980)$ (singlet), $f_0(1500)$ (octet), and $K_0^*(1430)$.

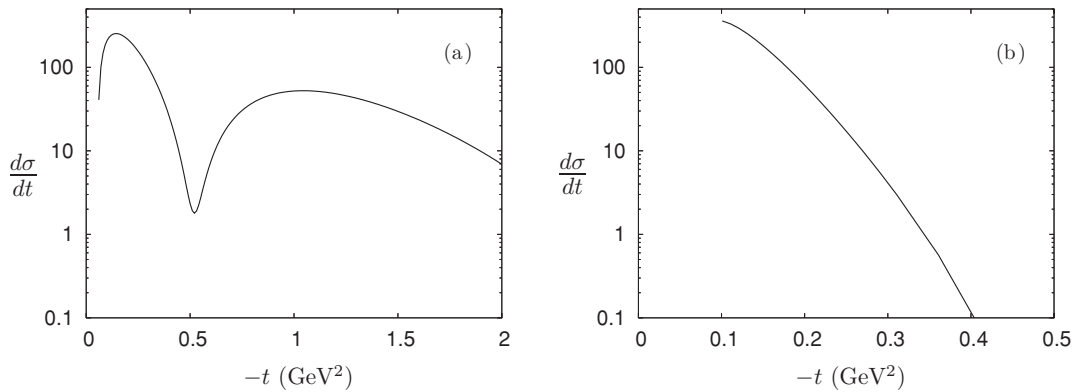


FIG. 2. Differential photoproduction cross sections in nb GeV⁻² for ground-state $a_0(1450)$ on (a) protons and (b) ${}^4\text{He}$ at $E_\gamma = 5$ GeV.

The $a_0(1450)$ is assigned to the 2^3P_0 radial excitation. The integrated cross sections for photoproduction of $a_0(980)$ and $f_0(980)$ on protons and ${}^4\text{He}$ at $E_\gamma = 5$ GeV are given in Table V, and the differential cross sections in Fig. 3. As for $a_0(1450)$ in scenario I, the cross section for photoproduction of the isovector $a_0(980)$ on ${}^4\text{He}$ is large. The large photoproduction cross sections for $a_0(980)$ and $f_0(980)$ in this scenario are a direct consequence of their being $n\bar{n}$ states. A corollary is that if $a_0(980)$ or $f_0(980)$ are non- $n\bar{n}$ states, as in scenario I, even a small $n\bar{n}$ admixture will lead to a significant increase in the cross section. The integrated cross sections for $f_0(1500)$ and $a_0(1450)$ are also given in Table V, and the differential cross sections on protons in Fig. 3.

3. Scenario III

As in scenario II, $a_0(980)$ and $f_0(980)$ are in the $n\bar{n}$ ground-state nonet, but $f_0(980)$ is no longer a singlet. The integrated cross section and differential cross section for $a_0(980)$ are as in Table V and Fig. 3, but the results for $f_0(980)$ in Table V and Fig. 3 need to be scaled up by a factor of 1.5. Both $a_0(1450)$ and $f_0(1500)$ are now members of the first radially excited nonet. The results for $a_0(1450)$ are as in Table V and Fig. 3(d). The integrated cross sections for the radially excited $f_0(1500)$ are 24.7 nb on protons and 0.4 nb on ${}^4\text{He}$. The differential cross section for $f_0(1500)$ on protons is shown in Fig. 4(a).

TABLE V. Scenario II. Integrated photoproduction cross sections in nb on protons and ${}^4\text{He}$ at $E_\gamma = 5$ GeV for $a_0(980)$, $f_0(980)$, $f_0(1500)$, and $a_0(1450)$ assuming that the isoscalars are members of the ground-state nonet, that $f_0(980)$ is pure singlet, $f_0(1500)$ is pure octet, and $a_0(1450)$ is the first radial excitation.

State	Proton	${}^4\text{He}$
$a_0(980)$	167.9	47.2
$f_0(980)$	91.0	3.5
$f_0(1500)$	35.4	0.6
$a_0(1450)$	21.4	4.7

4. Scenario IV

This scenario is analogous to scenario II with $f_0(1370)$ replacing $f_0(1500)$ as the octet member of the ground-state nonet. The integrated cross sections for photoproduction on protons and ${}^4\text{He}$ at $E_\gamma = 5$ GeV are 47 and 1.1 nb, respectively. The differential cross section at $E_\gamma = 5$ GeV is shown in Fig. 4(b).

IV. MASS DISTRIBUTIONS

We present results for the $\pi^0\pi^0$ channel for the isoscalars. Other pseudoscalar-pseudoscalar channels can be obtained from these by scaling using the branching fractions of Table VII, or the results of Bugg [21] for the special case of the $f_0(1370)$.

A. The signal

To obtain mass distributions for the $f_0(1370)$, $f_0(1500)$, $f_0(1710)$, and $a_0(1450)$, we represent them as relativistic Breit-Wigner resonances with energy-dependent partial widths. The signal cross section for the final state i is given by (see Appendix)

$$\frac{d\sigma}{dt dM} = \frac{d\sigma_0(t, M)}{dt} \frac{2m_S^2}{\pi} \frac{\Gamma_i(M)}{(m_S^2 - M^2)^2 + M^2\Gamma_{\text{Tot}}^2}, \quad (24)$$

where $d\sigma_0(t, M)/dt$ is the narrow-width differential cross section at a scalar mass M . For pseudoscalar-pseudoscalar final states, the partial width $\Gamma_i(M)$ is given in terms of the SPP coupling g_i by

$$\Gamma_i(M) = \frac{g_i^2 \rho(M, m_a, m_b)}{16\pi M}, \quad (25)$$

with

$$\rho(M, m_a, m_b) = \sqrt{[1 - (m_a + m_b)^2/M^2][1 - (m_a - m_b)^2/M^2]}, \quad (26)$$

where m_a and m_b are the masses of the two scalars. Conversely, g_i is determined from the partial width at resonance, putting $M = m_S$ in Eq. (25).

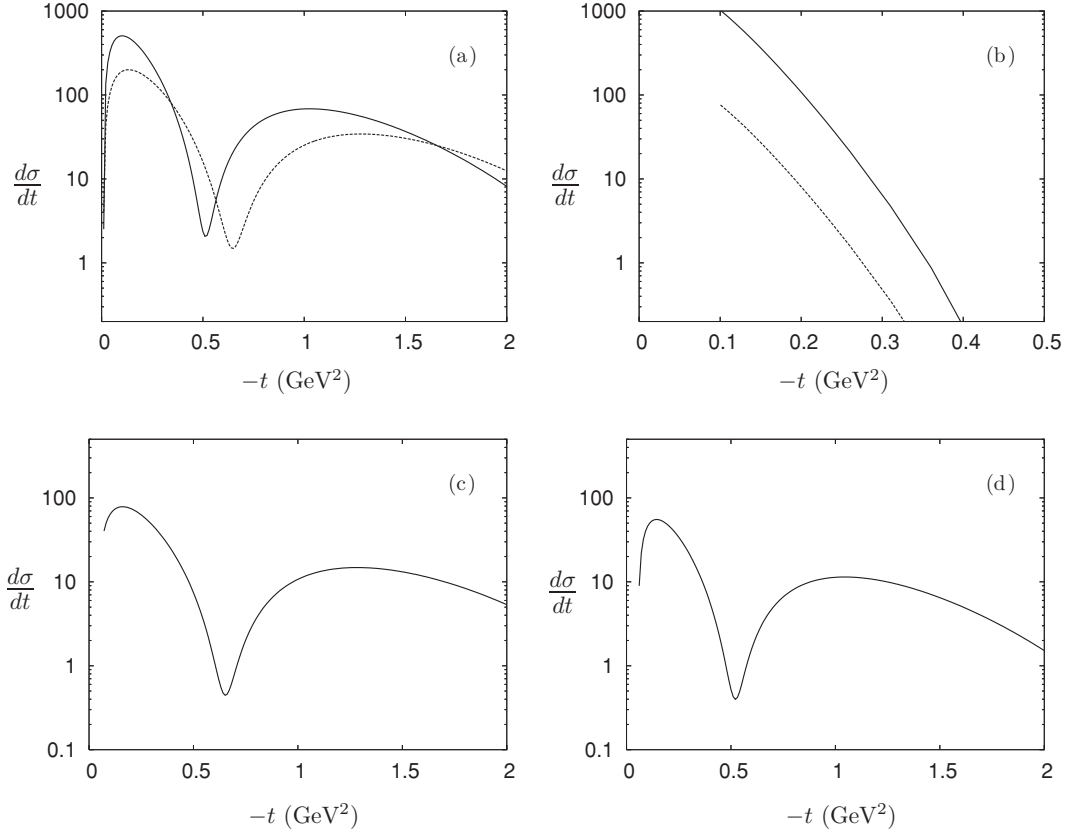


FIG. 3. Differential photoproduction cross sections in nb GeV⁻² on (a) protons and (b) ^4He for $a_0(980)$ (solid curves) and $f_0(980)$ (dashed curves) assuming that they are members of the ground-state nonet and that $f_0(980)$ is a pure singlet, and on protons (c) for $f_0(1500)$ assuming that it is a member of the ground-state nonet and is a pure octet and (d) for $a_0(1450)$ assuming it is in the first radial excitation.

The 4π channels $2\pi^+2\pi^-$, $\pi^+\pi^-2\pi^0$, and $4\pi^0$ represent a significant fraction of scalar decays and are dominated by $\rho\rho$ and $\sigma\sigma$. As we do not consider them explicitly, we represent them collectively using the parametrization of 4π phase space suggested by Bugg [21]:

$$\rho_{4\pi}(M) = \frac{\sqrt{1 - 16m_\pi^2/M^2}}{1 + \exp[-\Lambda(M^2 - M_0^2)]}, \quad (27)$$

with $M_0 = 1.799$ GeV and $\Lambda = 3.39$ GeV⁻². Then for the 4π states, we take

$$\Gamma_{4\pi} = \gamma_{4\pi} \frac{\rho_{4\pi}(M)}{\rho_{4\pi}(m_S)}, \quad (28)$$

so that $\gamma_{4\pi}$ is the 4π partial width at resonance.

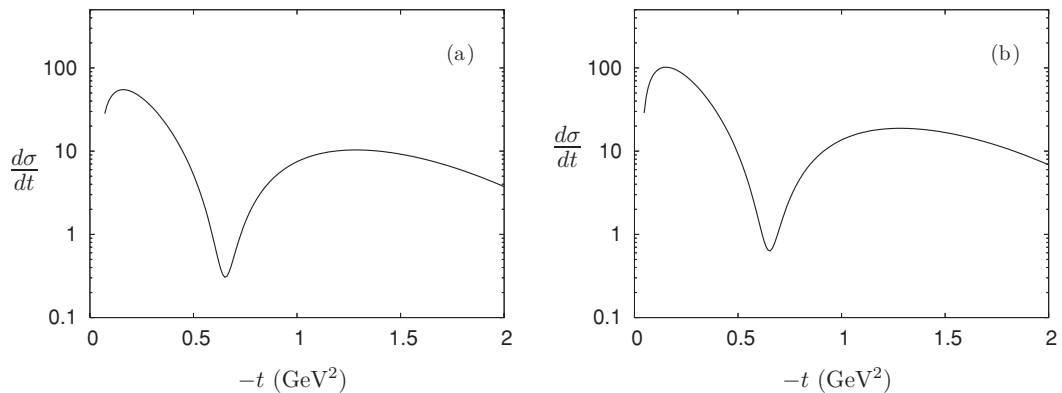


FIG. 4. Differential photoproduction cross sections on protons in nb GeV⁻² for (a) $f_0(1500)$ assuming that it is a member of the first radially excited nonet and (b) $f_0(1370)$ assuming it is the octet member of the ground-state nonet.

The total width is then

$$\Gamma_{\text{Tot}}(M) = \sum_i \Gamma_i(M). \quad (29)$$

Although the dominant decay of $f_0(980)$ is $\pi\pi$ and that of $a_0(980)$ is $\pi\eta$, both branching fractions being about 0.85 with the remainder in $K\bar{K}$ [1], these states reside at the $K\bar{K}$ threshold, so the procedure outlined above is not reliable. Instead, we use the Breit-Wigner parametrizations obtained in the analysis of ϕ radiative decays [39,40]. In this section, the “no-structure” versions of the fits are employed, which correspond to a point-like $\phi\gamma S$ vertex, and are in line with the quark-loop radiative transition assumption. The Breit-Wigner width takes the form

$$\Gamma(M) = g_{\pi\pi}^2 \frac{v_{\pi}(M)}{8\pi M^2} + g_{K\bar{K}}^2 \frac{v_{K^{\pm}}(M) + v_{K^0}(M)}{8\pi M^2}, \quad (30)$$

where $v_{\pi}(M) = \sqrt{M^2/4 - M_{\pi\pi}^2}$ and $v_K(M) = \sqrt{M^2/4 - M_{K\bar{K}}^2}$ are momenta with an analytical continuation below threshold. The corresponding parameters are $M = 0.9847$ GeV, $g_{K^+K^-} = g_{K^0\bar{K}^0} = 0.4$ GeV, and $g_{\pi^+\pi^-} = \sqrt{2}g_{\pi^0\pi^0} = 1.31$ GeV for $f_0(980)$; and $M = 0.983$ GeV, $g_{K^+K^-} = g_{K^0\bar{K}^0} = 1.57$ GeV, and $g_{\pi\eta} = 2.2$ GeV for $a_0(980)$.

To obtain mass distributions, it is necessary to have accurate branching fractions to hadronic final states. This is the case for $f_0(1500)$ but not for $f_0(1370)$ or $f_0(1710)$, particularly the former [1,18,19,21,22]. The various hadronic decay channels of $f_0(1500)$ are well defined. This is illustrated in Table VI in which the branching fractions, in percent, are given from the PDG [1], the WA102 experiment [41] as obtained in the analysis of Close and Kirk [7], and the crystal barrel experiment [42]. The usefulness of $a_0(1450)$ as a check on the model is also compromised by the limited information on the hadronic branching fractions [1], which we discuss below.

For definiteness, we use the results of the WA102 Collaboration [41] for the isoscalars. These comprise a complete data set for the decay of $f_0(1370)$, $f_0(1500)$, and $f_0(1710)$ to all pseudoscalar meson pairs. As only relative branching ratios are provided, to obtain the absolute branching ratios that we require, we use the analysis of these data in Ref. [7] to take account of other channels. The branching fractions to pseudoscalars are summarized in Table VII. Of course, for the $\pi^0\pi^0$ channel, the $\pi\pi$ branching fraction shown has to be divided by a factor of 3. We also take the results of the WA102 Collaboration [41] for the total widths: 272 ± 50 MeV for $f_0(1370)$, 108 ± 18 for $f_0(1500)$, and 124 ± 24 for $f_0(1710)$.

TABLE VI. Branching fractions in percent for $f_0(1500)$ from the PDG [1], the WA102 experiment [41] from the analysis of Close and Kirk [7] (CK), and the crystal barrel experiment [42] (CB).

Channel	PDG	WA102/CK	CB
$\pi\pi$	34.9 ± 2.3	33.7 ± 3.4	33.9 ± 3.7
$\eta\eta$	5.1 ± 0.9	6.1 ± 0.1	2.6 ± 0.3
$\eta\eta'$	1.9 ± 0.8	3.2 ± 0.7	2.2 ± 0.1
$K\bar{K}$	8.6 ± 0.1	10.7 ± 2.4	6.2 ± 0.5
4π	49.5 ± 3.3	46.3 ± 8.5	55.1 ± 16.9

TABLE VII. Branching fractions for the scalars from Refs. [41] and [7].

State	$\pi\pi$	$K\bar{K}$	$\eta\eta$	$\eta\eta'$
$f_0(1370)$	0.027	0.013	0.004	
$f_0(1500)$	0.337	0.107	0.061	0.032
$f_0(1710)$	0.119	0.595	0.286	

We see from Table VII that the branching fractions of $f_0(1370)$ to pseudoscalars are small, the principal decay mode being to 4π [42]. However, there is a major disagreement with the $\pi\pi$ branching fraction shown in Table VII. In the analysis of Bugg [21], the $2\pi : 4\pi$ ratio at resonance is given as 6:1. The results of Albaladejo and Oller [22] imply that the three pseudoscalar channels $\pi\pi$, $\eta\eta$, and $K\bar{K}$ saturate the decay modes of $f_0(1370)$ with $\pi\pi$ dominant. The consequences of this alternative view of the $f_0(1370)$ are discussed where appropriate.

The relative branching fractions $\pi\eta'(980)/\pi\eta$ and $K\bar{K}/\pi\eta$ of the $a_0(1450)$ are 0.35 ± 0.16 and 0.88 ± 0.23 , respectively [1]. However, the dominant decay mode of $a_0(1450)$ appears to be $\omega\pi\pi$ [43], although there is some uncertainty in the actual branching fraction [1]. Relative to $\pi\eta$, it is quoted as 10.7 ± 2.3 , obtained by comparing the total rates of $p\bar{p} \rightarrow a_0(1450)\pi$ for $a_0(1450) \rightarrow \pi\eta$ and $a_0(1450) \rightarrow \omega\pi^+\pi^-$ and assuming the $\omega\pi\pi$ final state is $\omega\rho$. The uncertainty is also reflected in the width; so as the $a_0(1450)$ is peripheral to our argument, we do not show any mass distributions but simply note that the cross section for $a_0(1450)$ photoproduction is sufficiently large for it to be used to clarify the $a_0(1450)$ decay modes.

1. Scenario I

The $\pi^0\pi^0$ mass distributions $d\sigma/dM$ for $f_0(1370)$, $f_0(1500)$, and $f_0(1710)$ are given in Fig. 5, in each case for light, medium, and heavy glueball masses and using the branching fractions of Table VII. Note the difference in scale in Fig. 5(c), reflecting the small $\pi\pi$ branching fraction for $f_0(1370)$ and the small cross section for $f_0(1710)$. However, if the $\pi\pi$ branching fraction of $f_0(1370)$ from the analysis of Refs. [21,22] is used instead of that in Table VII, the mass distribution is about a factor of 30 larger. The distortion of the Breit-Wigner line shape for $f_0(1370)$ arises primarily from the combined effect of the small $\pi\pi$ branching fraction and the large, rapidly rising 4π channel in the denominator. As $f_0(980)$ and $a_0(980)$ are not $n\bar{n}$ states in this scenario, discussion of them is deferred to Sec. V, where the extreme possibility of a purely molecular assignment is considered.

2. Scenario II

The $a_0(980)$, $f_0(980)$, and $f_0(1500)$ are members of the ground-state nonet with $f_0(980)$ and $f_0(1500)$ mixed such that the former is a singlet and the latter is an octet. The $\pi^0\pi^0$ and $\pi^0\eta^0$ mass distributions for $f_0(980)$ and $a_0(980)$ are shown in

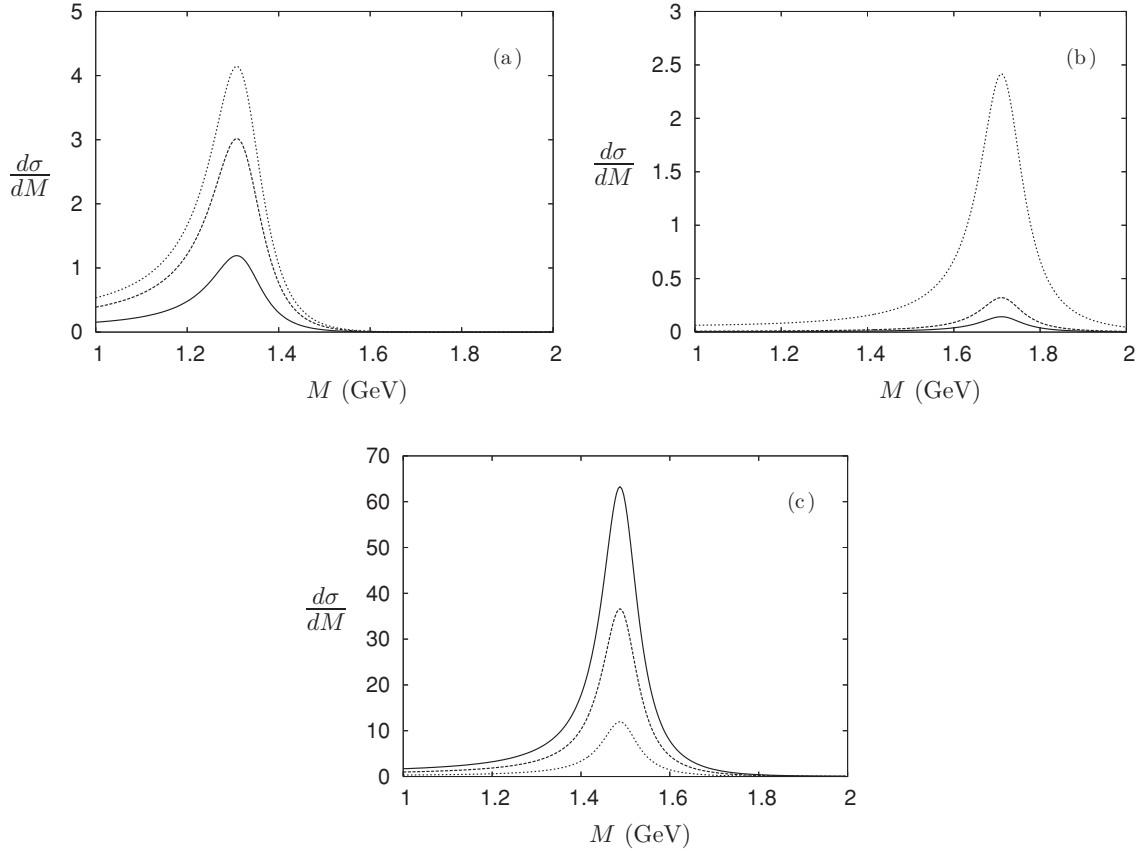


FIG. 5. Scenario I. Differential $\pi^0\pi^0$ mass distributions in nb GeV^{-1} at $E_\gamma = 5 \text{ GeV}$ for (a) $f_0(1370)$, (b) $f_0(1710)$, and (c) $f_0(1500)$. The glueball masses are L (solid), M (dashed), and H (dotted) in each figure.

Figs. 6(a) and 6(b), respectively. The $\pi^0\pi^0$ mass distribution for $f_0(1500)$ is given as the solid curve in Fig. 7(a). $f_0(1370)$ does not exist in this scenario.

should be scaled up by a factor of 1.5. $f_0(1500)$ is now a member of the first radial excitation, and the corresponding $\pi^0\pi^0$ mass distribution is shown as the dashed curve in Fig. 7(a). $f_0(1370)$ does not exist in this scenario.

3. Scenario III

The $a_0(980)$ and $f_0(980)$ are as in scenario II, although the latter is no longer a singlet, so the $\pi^0\pi^0$ mass distribution

4. Scenario IV

This is analogous to scenario II, but the octet member is $f_0(1370)$. The $\pi^0\pi^0$ mass distribution is given in Fig. 7(b)

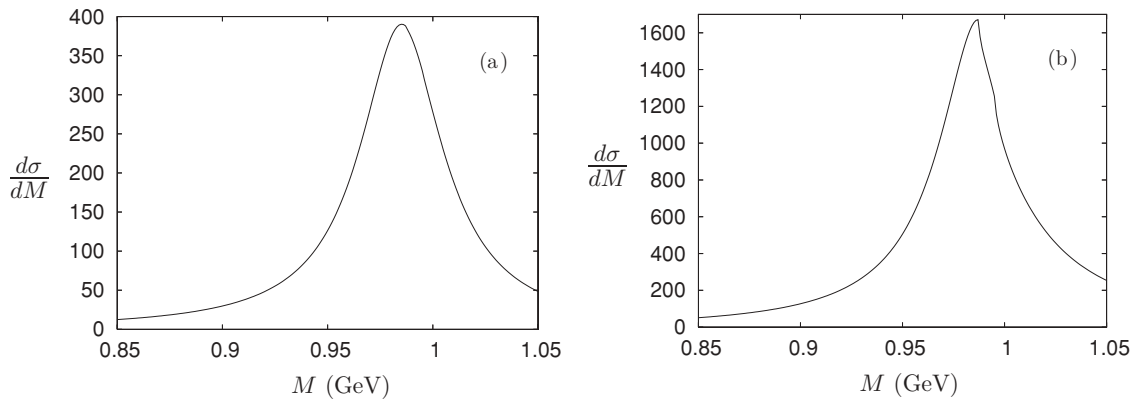


FIG. 6. Scenario II. (a) Differential $\pi^0\pi^0$ mass distribution in nb GeV^{-1} for $f_0(980)$ at $E_\gamma = 5 \text{ GeV}$. (b) Differential $\pi^0\eta^0$ mass distribution in nb GeV^{-1} for neutral $a_0(980)$ at $E_\gamma = 5 \text{ GeV}$.

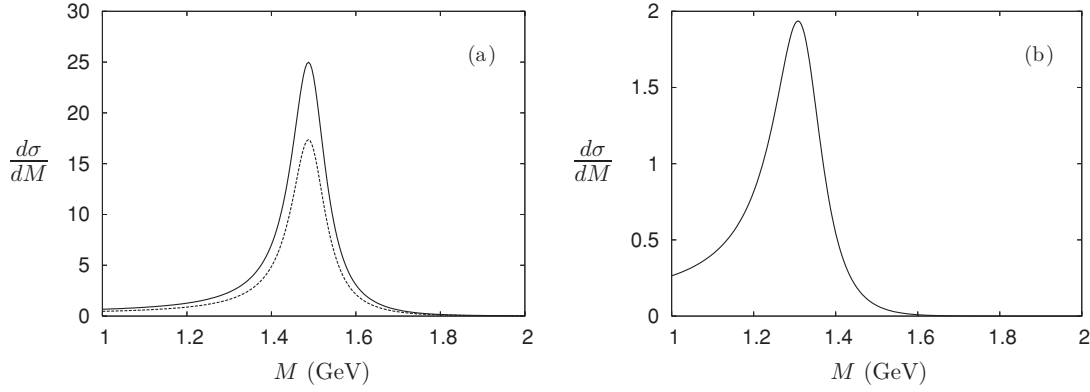


FIG. 7. Scenarios III and IV. (a) Differential $\pi^0\pi^0$ mass distributions in nb GeV⁻¹ at $E_\gamma = 5$ GeV for $f_0(1500)$ as an octet ground state (solid) and as a member of the first radial excitation (dashed). (b) Differential $\pi^0\pi^0$ mass distribution in nb GeV⁻¹ at $E_\gamma = 5$ GeV for $f_0(1370)$ as an octet ground state.

using the branching fraction of Table VII. Recall that if the $\pi\pi$ branching fraction of the $f_0(1370)$ from the analysis of Refs. [21,22] is used instead of that in Table VII, the mass distribution is about a factor of 30 larger. $f_0(1500)$ and $f_0(1710)$ are considered to be unmixed glueballs so cannot be photoproduced directly.

B. Continuum background

There is a coherent, continuum background in the $\pi^0\pi^0$, $\pi^0\eta^0$, and $\eta^0\eta^0$ channels. The production mechanism is illustrated in Fig. 8.

Each graph has the form

$$M_\mu = g_1 g_2 \epsilon_{\mu\rho\beta\gamma} q_\beta v_\gamma \epsilon_{\rho\nu\lambda\sigma} p_\lambda v_\sigma F_\nu D(s, t) \Pi(v). \quad (31)$$

As before, q is the photon momentum, $p = p_1 - p_2$ where p_1 and p_2 are the initial and final proton momenta, and $v = k - q$ where k is the momentum of the pseudoscalar in the upper vertex. F_ν is given by Eq. (1), $D(s, t)$ is the Regge propagator from Eq. (19), and

$$\Pi(v) = \frac{1}{m_v^2 - v^2 - im_v\Gamma_v}, \quad (32)$$

where m_v and Γ_v are the mass and width of the vector meson in the upper half of the graph. The quantities g_1, g_2 are,

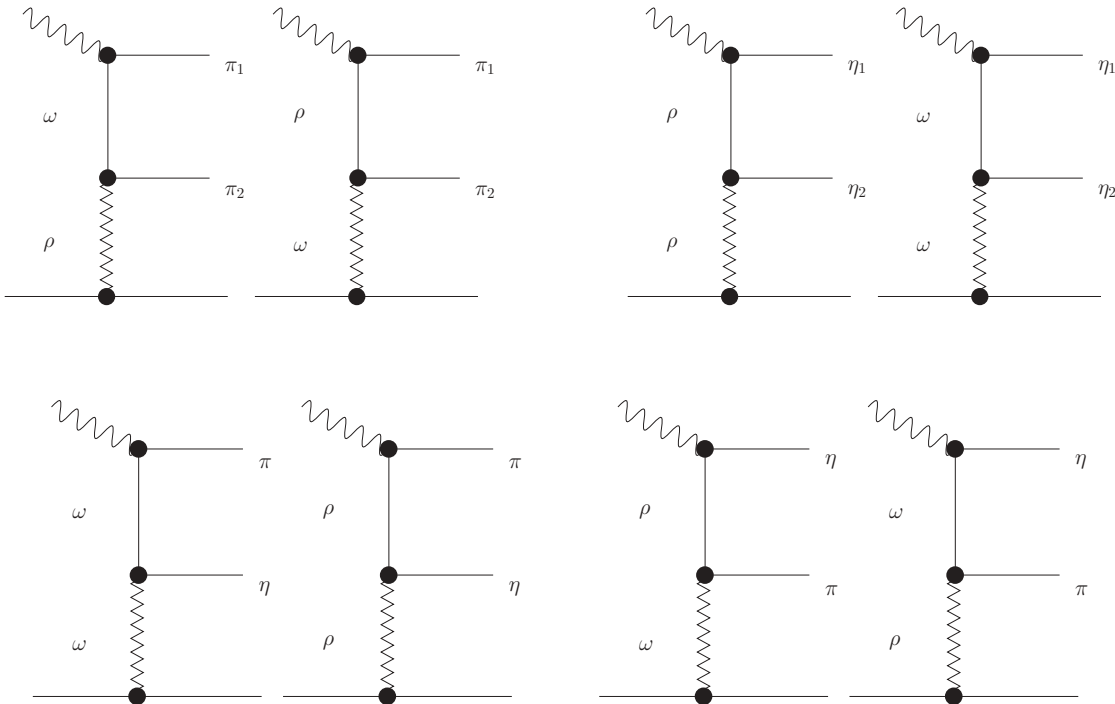


FIG. 8. Feynman diagrams for continuum $\pi^0\pi^0$, $\eta^0\eta^0$, and $\pi^0\eta^0$ photoproduction. In addition, there are diagrams with $\pi_1 \leftrightarrow \pi_2$ and $\eta_1 \leftrightarrow \eta_2$ for the first two.

respectively, the γ - P_1 - V_1 and V_1 - P_2 - V_2 coupling constants at the top and middle vertices of the diagrams.

The product of the coupling constants $g_1 g_2 \equiv C g_0$, where g_0 can be estimated from Ref. [44] as

$$g_0 = \frac{G^2 e}{g\sqrt{2}}, \quad G = \frac{3\sqrt{2}g^2}{4\pi^2 f}, \quad (33)$$

with $g = 4.2$ and $f = 132$ MeV, giving $(1.514 \times 10^4) \alpha_{\text{em}} \text{ GeV}^{-2}$. The constant $C = C_{V_2 P_1 P_2}$ is the appropriate Clebsch-Gordan coefficient,

$$\begin{aligned} 1 &= C_{\rho\pi\pi} = 3C_{\omega\pi\pi} = 3\sqrt{\frac{3}{2}}C_{\rho\pi\eta} \\ &= \sqrt{\frac{3}{2}}C_{\omega\pi\eta} = \frac{3}{2}C_{\rho\eta\eta} = \frac{9}{2}C_{\omega\eta\eta}. \end{aligned} \quad (34)$$

The explicit calculation is given in the Appendix, and the results for $\pi^0\pi^0$, $\pi^0\eta^0$, and $\eta^0\eta^0$ are shown in Fig. 9. This continuum background is sufficiently large that it must be taken into account in any analysis of scalar photoproduction, and this is the primary reason for including it. There are, of course, additional continuum background contributions from reactions such as $\gamma p \rightarrow \Delta(1232)\pi$, $\gamma p \rightarrow \Delta(1232)\eta$, and $\gamma p \rightarrow N(1535)\pi$ that are less amenable to calculation but must also be taken into account in the analysis.

C. Interference

In any experimental environment, the interference pattern will be complicated. In addition to interference between a given scalar and the continuum background, there will be interference among the scalars themselves. Accordingly, we restrict discussion to a simple illustrative example.

The formula for the cross section describing the interference between direct production of a single scalar, as in Sec. III, and the continuum background is given in the Appendix. The results for $f_0(1500)$ in scenario I, for constant relative phases of 0° , 90° , 180° , and 270° , are given in Fig. 10.

V. MESON LOOP MECHANISM

As we already mentioned in the Introduction, radiative transitions of scalars can also proceed via intermediate meson loops. This is widely discussed in connection with the possibility of scalar resonances generated dynamically. Indeed, if the scalars contain significant admixtures of compact quark states, then both quark loops and meson loops contribute to the radiative transition amplitude, while in the case of dynamically generated resonances (molecules), only meson loops contribute.

The most well-studied case is transition via loops of charged pseudoscalars, in which case the γ SV vertex takes the form

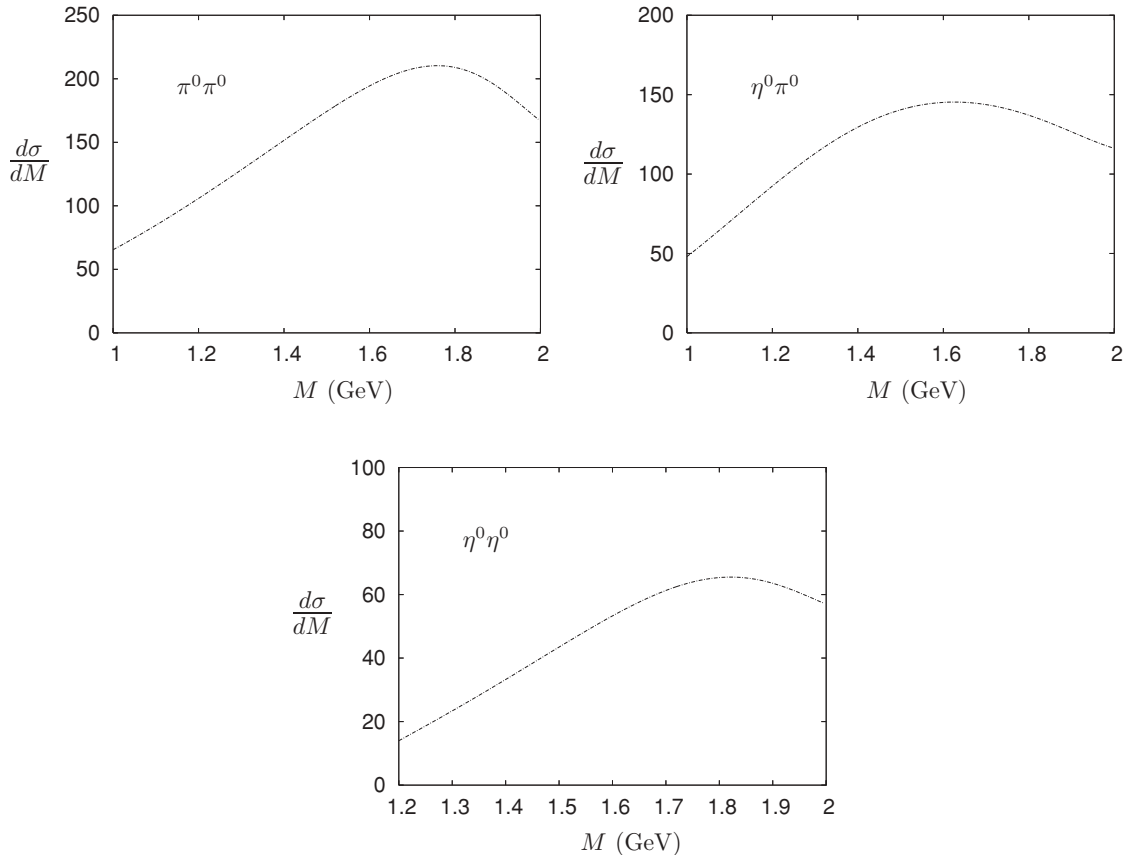


FIG. 9. Continuum $\pi^0\pi^0$, $\pi^0\eta^0$, and $\eta^0\eta^0$ backgrounds in nb GeV^{-1} .

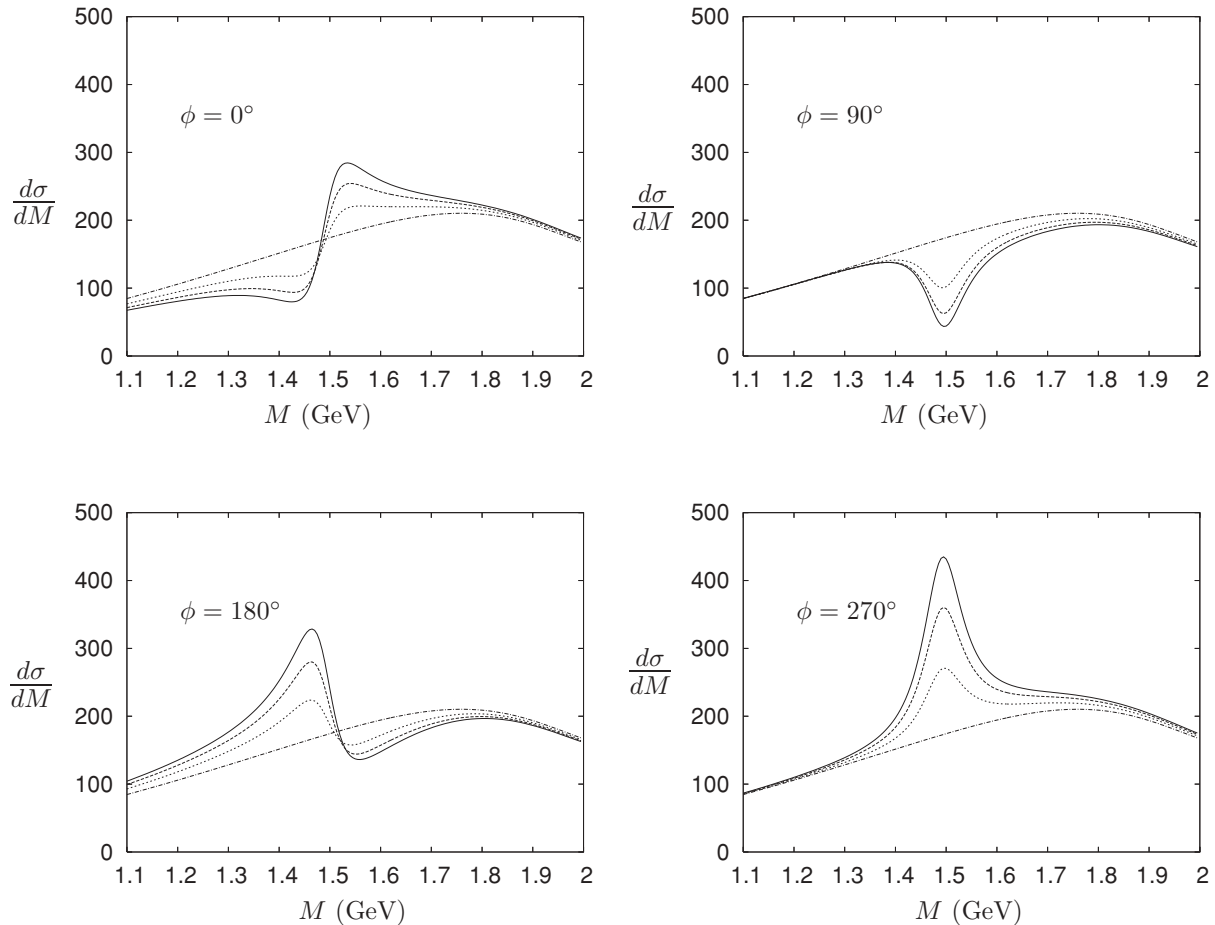


FIG. 10. Interference cross section in nb GeV^{-1} between the $\pi^0\pi^0$ continuum background and $f_0(1500)$ for different values of the relative phase ϕ in scenario I. The glueball masses are L (solid), M (dotted), and H (dashed) in each figure.

of Eq. (1) with the coupling $g_S(m_S^2, m_V^2)$ given by

$$g_S(m_S^2, m_V^2) = e \frac{g_{PPV} g_{PPS}}{2\pi^2 m_P} I_P(a, b), \quad (35)$$

where $a = m_V^2/m_P^2$, $b = m_S^2/m_P^2$, m_P is the mass of the pseudoscalar in the loop, and g_{PPV} and g_{PPS} are the VP^+P^- and SP^+P^- coupling constants. The explicit expression for the loop integral function $I_P(a, b)$ is given in the Appendix.

As shown in Ref. [28], the decay rates involving $f_0(980)$ and $a_0(980)$ exhibit a distinct hierarchy pattern: the closer the mass of the vector meson to the $K\bar{K}$ threshold, the larger is the contribution of the kaon loop. So the intermediate kaon-loop mechanism should dominate the $\phi \rightarrow \gamma S$ decay amplitude, as suggested in Ref. [45]. The estimates [28] for scalar radiative widths in the $K\bar{K}$ molecular model for scalars are

$$\Gamma(a_0/f_0 \rightarrow \gamma\rho/\omega) \approx 3 \text{ keV}, \quad (36)$$

in contrast to the quark-loop results of Table II. Thus the decays $a_0/f_0 \rightarrow \gamma\rho/\omega$ provide strong discrimination between models for these scalars.

In scenario I, $a_0(980)$ and $f_0(980)$ are not $n\bar{n}$ states. In this section, we consider the extreme possibility of a pure molecular assignment for them, in which case the relevant photoproduction mechanism is via a meson loop. The

calculation of the $a_0(980)$ cross section is straightforward, as only the kaon loop contributes. In the $f_0(980)$ case, there is also a contribution from the $\pi^+\pi^-$ loop. The photoproduction formalism is presented in the Appendix, and mass distributions are shown in Fig. 11. The integrated cross sections are 1.3 nb for $f_0(980)$ and 0.5 nb for $a_0(980)$. As expected, these cross sections are small, in accordance with the general arguments given in Ref. [28].

Recently the contribution of intermediate vector meson channels to scalar radiative decays has been considered [46,47]. In particular, non-negligible contributions to the $a_0(980) \rightarrow \gamma\omega$ [46] and $f_0(1710) \rightarrow \gamma\rho$ [47] amplitudes were obtained. There is, however, an important difference between a purely pseudoscalar loop and one with vector mesons. The former amplitude is finite (see the discussion in Refs. [48,49]), while the latter diverges logarithmically and a cutoff is needed. It is claimed in Refs. [46,47] that this divergence can be properly treated, though the details of the cutoff dependence are not given there.

In the photoproduction context, including intermediate vector mesons corresponds to taking into account final-state interactions in the background graphs of Fig. 9 (and including K and K^* mesons in the loop). The $\pi^+\pi^-$ and K^+K^-S -wave photoproduction has been treated in Ref. [50] in such an

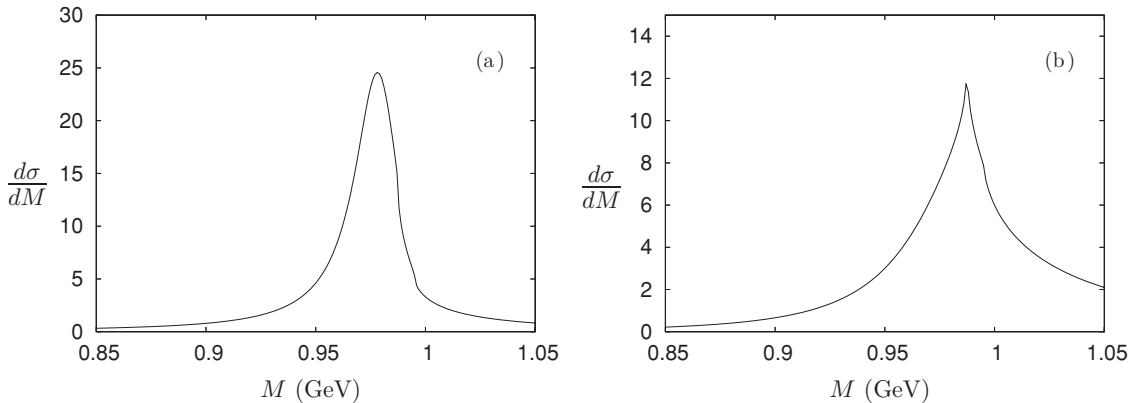


FIG. 11. (a) Differential $\pi^0\pi^0$ mass distribution in nb GeV^{-1} at $E_\gamma = 5$ GeV for $f_0(980)$ in the pseudoscalar loop model. (b) Differential $\pi^0\eta$ mass distribution in nb GeV^{-1} at $E_\gamma = 5$ GeV for $a_0(980)$ in the pseudoscalar loop model.

approach. Corresponding contributions are to be taken into account in the analysis of the photoproduction of neutral pairs as well, because they are potentially important.

VI. CONCLUSIONS

It is clear that light-quark scalar meson photoproduction on protons is a practical proposition given the luminosities available to modern photoproduction. Although we have limited the discussion to neutral pseudoscalar-pseudoscalar final states, most of the cross sections we have obtained are sufficiently large to allow a limited acceptance for these channels. Unfortunately, the cross sections on ${}^4\text{He}$ are small for the isoscalars, because their dominant radiative decay is to $\rho\gamma$. Of course, for the isovectors, with their dominant radiative decay being to $\omega\gamma$, the cross sections for photoproduction on ${}^4\text{He}$ are comparable to those on protons.

To resolve all the issues discussed in the Introduction requires obtaining the photoproduction cross section for at least two scalars, but there are exceptions. In two cases, the difference between different models for a particular scalar is so great that the issue can be settled by measuring the cross section for that scalar alone.

The first of these is the question of the natures of $a_0(980)$ and $f_0(980)$, in particular whether there is a significant or even dominant $n\bar{n}$ component in their wave function. The full $n\bar{n}$ cross section is given in Table V, and an estimate of the non- $n\bar{n}$ cross section in Sec. V. Both $a_0(980)$ and $f_0(980)$ have been observed in photoproduction: at CLAS [38] with quasi-real photons from a 5.75 GeV electron beam and at CB-ELSA at γp center-of-mass energies up to 2.55 GeV [51,52]. The CLAS data have not been fully analyzed, but $\pi^0\eta$ and $\pi^0\pi^0$ mass plots (not acceptance corrected) show clear evidence for $a_0(980)$ and $f_0(980)$, respectively. Preliminary results from ELSA also show evidence for $a_0(980)$ [51] and $f_0(980)$ [52] photoproduction at the upper end of their energy ranges. These data point to an admixture of $n\bar{n}$ in the $a_0(980)$ and $f_0(980)$ wave functions. Given the small cross section anticipated in the molecular model, even a modest admixture of $n\bar{n}$ in the wave function will dominate the cross section.

As there are no microscopic calculations of the $V S \gamma$ couplings with $V = \rho, \omega$ in the chiral Lagrangian models [9–15] which involve $q\bar{q}, qq\bar{q}\bar{q}$ mixing, we cannot comment quantitatively on this variation despite its undoubted importance. The desirability of such calculations in the context of four-quark chiral models has been stressed in Ref. [13]. However, qualitatively we can say that our general conclusion does not change: scalar meson photoproduction is a powerful tool for resolving the problem of the isoscalars.

$f_0(1370)$ provides the second case in which measuring the cross section would resolve the issue of its $\pi\pi$ branching fraction and possibly also the issue of its existence. The cross section for $f_0(1370)$ photoproduction at $E_\gamma = 5$ GeV varies from scenario to scenario. In scenarios II and III, $f_0(1370)$ does not exist. In scenario I, the cross section varies from 27 to 94 nb as the glueball mass varies from light to heavy; and in scenario IV, as the octet member of the ground-state nonet, the cross section is 140 nb. So the nonzero cross sections vary by a factor of 5. The conventional branching fraction is 2.7%, but in the analyses of Refs. [21,22] it is closer to 80%, which is a factor of 30 larger. So for a $\pi\pi$ branching fraction of 2.7%, the cross section times the $\pi^0\pi^0$ branching fraction lies in the range 0.24–1.26 nb, while for a $\pi\pi$ branching fraction of 80% the range is 7.2–37.3 nb. The CLAS $\pi^0\pi^0$ data cover this mass range and so, in principle, could be used.

For $f_0(1500)$, the photoproduction cross sections in various scenarios are very similar, so it is not necessarily possible to use $f_0(1500)$ by itself to resolve the ambiguities surrounding the nature of the scalars. The cross sections in scenario I with a heavy glueball is 17 nb; in scenario II, as the octet member of the ground-state nonet, it is 35 nb; and in scenarios III and IV, as a member of the first radial excitation, the cross section is 25 nb, although this should probably be considered as an upper limit due to its sensitivity to the wave functions. However in scenario I, if the glueball mass is in the light to medium range, with cross sections of 90 and 52 nb, respectively, then a clear result can be obtained. Otherwise, results for $f_0(1500)$ must be combined with those for $f_0(980)$ or $f_0(1370)$.

In principle, photoproduction of $a_0(1450)$ can also provide some discrimination, since the cross section as a member of the ground-state nonet (98 nb) is nearly a factor of 5 larger than that

as a member of the first radial excitation (21 nb). Unfortunately, the considerable uncertainty in the branching fractions [1] does not make this feasible at present. However, some information on $a_0(1450)$ photoproduction could, in principle, be obtained from the CLAS $\pi^0\eta^0$ data, because they cover the relevant mass range.

Because of the large 4π branching fraction of $f_0(1370)$ (with the conventional values) and $f_0(1500)$ and the implied large 5π branching fraction of $a_0(1450)$, if measurement of these channels were technically feasible then this would not only add to our information about the scalars but would assist in resolving their nature.

ACKNOWLEDGMENTS

We are grateful to Marco Battaglieri, David Bugg, Eberhard Klempt, Wolfgang Ochs, and Ulrike Thoma for helpful and informative discussions. Yu.S.K. acknowledges the support of the Federal Agency for Atomic Energy of the Russian Federation (Grants RFFI-05-02-04012-NNIOa, DFG-436 RUS113/820/0-1(R), and Nsh-4961.2008.2) and the Federal Program of the Russian Ministry of Industry, Science, and Technology (No. 40.052.1.1.1112).

APPENDIX

A. Narrow-width cross section

To obtain formula (17), note that we can write

$$A_{\mu\nu}\gamma_\nu + B_\mu = M_{\mu\nu}(a\gamma_\nu + bp_{1\nu}) = aM_{\mu\nu}\gamma_\nu + bN_\mu, \quad (\text{A1})$$

with

$$M_{\mu\nu} = g_{\mu\nu}(q \cdot p) - p_\mu q_\nu, \quad N_\nu = M_{\mu\nu}p_{1\nu}. \quad (\text{A2})$$

The required trace is

$$\begin{aligned} T_C &= \frac{1}{4} \text{Tr} \{(\gamma \cdot p_2 + m_p) \\ &\quad \times (aM_{\mu\lambda}\gamma_\lambda + bN_\mu)(\gamma \cdot p_1 + m_p)(a^*M_{\mu\nu}\gamma_\nu + b^*N_\mu)\} \\ &= \frac{1}{4}aa^*M_{\mu\lambda}M_{\mu\nu} \text{Tr} \{(\gamma \cdot p_2 + m_p)\gamma_\lambda(\gamma \cdot p_1 + m_p)\gamma_\nu\} \\ &\quad + \frac{1}{4}a^*bN_\mu M_{\mu\nu} \text{Tr} \{(\gamma \cdot p_2 + m_p)(\gamma \cdot p_1 + m_p)\gamma_\nu\} \\ &\quad + \frac{1}{4}ab^*M_{\mu\lambda}N_\mu \text{Tr} \{(\gamma \cdot p_2 + m_p)\gamma_\lambda(\gamma \cdot p_1 + m_p)\} \\ &\quad + \frac{1}{4}bb^*N_\mu N_\mu \text{Tr} \{(\gamma \cdot p_2 + m_p)(\gamma \cdot p_1 + m_p)\}. \end{aligned} \quad (\text{A3})$$

The basic traces entering Eq. (A3) are

$$\begin{aligned} &\frac{1}{4} \text{Tr} \{(\gamma \cdot p_2 + m_p)\gamma_\lambda(\gamma \cdot p_1 + m_p)\gamma_\nu\} \\ &= g_{\lambda\nu}(m_p^2 - p_1 \cdot p_2) + p_{2\lambda}p_{1\nu} + p_{1\lambda}p_{2\nu}, \\ &\frac{1}{4} \text{Tr} \{(\gamma \cdot p_2 + m_p)\gamma_\lambda(\gamma \cdot p_1 + m_p)\} \\ &= m_p(p_{1\lambda} + p_{2\lambda}), \\ &\frac{1}{4} \text{Tr} \{(\gamma \cdot p_2 + m_p)(\gamma \cdot p_1 + m_p)\} \\ &= m_p^2 + p_1 \cdot p_2. \end{aligned} \quad (\text{A4})$$

Inserting Eq. (A4) into Eq. (A3) gives

$$\begin{aligned} T_C &= aa^*[(m_p^2 - (p_1 \cdot p_2))M_{\mu\nu}M_{\mu\nu} + 2N_\mu N_\mu] \\ &\quad + 2m_p(a^*b + ab^*)N_\mu N_\mu \end{aligned}$$

$$+ (m_p^2 + (p_1 \cdot p_2))bb^*N_\mu N_\mu. \quad (\text{A5})$$

Equation (A5) can be rewritten in terms of invariants as

$$\begin{aligned} aa^* \{ &\frac{1}{2}s^2t + \frac{1}{2}st(t - 2m_p^2 - m_s^2) + \frac{1}{4}[2m_p^4t + t(t - m_s^2)^2 \\ &+ m_p^2(-2tm_s^2 + 2m_s^4)] \} + (ab^* + a^*b)[m_p s^2t \\ &+ m_p st(-2m_p^2 + t - m_s^2) + m_p^3(m_p^2t - m_s^2t + m_s^4)] \\ &+ bb^*(4m_p^2 - t)\frac{1}{8}[s^2t - st(2m_p^2 - t + m_s^2) \\ &+ m_p^2(m_p^2t - m_s^2t + m_s^4)]. \end{aligned} \quad (\text{A6})$$

The result (A6) can be written compactly in terms of the kinematical boundaries t_1 and t_2 given by

$$\begin{aligned} t_{1,2} &= \frac{1}{2s} [- (m_p^2 - s)^2 + m_s^2(m_p^2 + s) \\ &\quad \pm (m_p^2 - s)\sqrt{(m_p^2 - s)^2 - 2m_s^2(m_p^2 + s) + m_s^4}], \end{aligned} \quad (\text{A7})$$

so that for the exchange of a single vector meson

$$\begin{aligned} |M(s, t)|^2 &= -T_C = -\frac{1}{2}aa^*[s(t - t_1)(t - t_2) + \frac{1}{2}st(t - m_s^2)^2] \\ &\quad - \frac{1}{2}(ab^* + a^*b)m_p s(t - t_1)(t - t_2) \\ &\quad - \frac{1}{8}bb^*s(4m_p^2 - t)(t - t_1)(t - t_2). \end{aligned} \quad (\text{A8})$$

Finally, the differential cross section is given by

$$\frac{d\sigma}{dt} = -\frac{T_C}{16\pi(s - m_p^2)^2}. \quad (\text{A9})$$

Obviously, in practice the amplitudes for ρ and ω exchange are added coherently.

B. Signal cross section

The differential cross section for the production of a scalar, mass M , and its decay to two pseudoscalars, masses m_a and m_b , is

$$\frac{d\sigma_S}{dt dM d\Omega} = -\frac{1}{28\pi^4} \frac{k_i(M, m_a, m_b)}{(s - m_p^2)^2} T_S. \quad (\text{A10})$$

with

$$\begin{aligned} k_i(M, m_a, m_b) &= \sqrt{[M^2 - (m_a + m_b)^2][M^2 - (m_a - m_b)^2]}/2M \end{aligned}$$

Following Eq. (A5), T_S is

$$\begin{aligned} T_S &= a_S a_S^* \{ [m_p^2 - (p_1 \cdot p_2)] M_{\mu\nu} M_{\mu\nu} + 2N_\mu N_\mu \} \\ &\quad + 2m_p(a_S b_S^* + b_S a_S^*) N_\mu N_\mu \\ &\quad + [m_p^2 + (p_1 \cdot p_2)] b_S b_S^* N_\mu N_\mu, \end{aligned} \quad (\text{A11})$$

with

$$\begin{aligned} a_S &= \frac{g_i}{m_S^2 - M^2 - iM\Gamma_{\text{Tot}}} [g_{S\rho}(g_{V\rho} + 2m_p g_{T\rho})D_\rho \\ &\quad + g_{S\omega}(g_{V\omega} - 2m_p g_{T\omega})D_\omega], \\ b_S &= -\frac{g_i}{m_S^2 - M^2 - iM\Gamma_{\text{Tot}}} (2g_{S\rho} g_{T\rho} D_\rho + 2g_{S\omega} g_{T\omega} D_\omega). \end{aligned} \quad (\text{A12})$$

Both ρ and ω exchanges have been included explicitly, and D_ρ, D_ω are the Regge propagators. The decay constant g_i in Eq. (A12) is defined in terms of the partial width Γ_i at resonance by

$$\Gamma_i = \frac{g_i^2 \rho_i(m_S, m_a, m_b)}{16\pi m_S}, \quad (\text{A13})$$

with

$$\begin{aligned} \rho_i(M, m_a, m_b) &= \sqrt{[1 - (m_a + m_b)^2/M^2][1 - (m_a - m_b)^2/M^2]} \\ &= 2k_i(M, m_a, m_b)/M. \end{aligned} \quad (\text{A14})$$

Substituting Eq. (A13) into Eq. (A12) and recalling Eq. (A9) gives

$$\frac{d\sigma}{dt dM} = \frac{d\sigma_0(t, M)}{dt} \frac{2m_S^2}{\pi} \frac{\Gamma_i(M)}{(m_S^2 - M^2)^2 + M^2\Gamma_{\text{Tot}}^2}, \quad (\text{A15})$$

where $d\sigma_0(t, M)/dt$ is the narrow-width cross section at the scalar mass M .

C. Background cross section

First note the simplification of Eq. (31), that is,

$$\begin{aligned} \epsilon_{\mu\rho\beta\gamma} q_\beta v_\gamma \epsilon_{\rho\nu\lambda\sigma} p_\lambda v_\sigma &= -g_{\mu\nu}[(q \cdot p)v^2 - (q \cdot v)(v \cdot p)] \\ &\quad - v_\mu[q_\nu(p \cdot v) - v_\nu(q \cdot p)] \\ &\quad - p_\mu[v_\nu(q \cdot v) - q_\nu v^2], \end{aligned} \quad (\text{A16})$$

and define, with $i = 1, 2$,

$$\begin{aligned} M_{\mu\nu}^{(i)} &= g_{\mu\nu}b_i + v_{i\mu}c_{i\nu} + p_\mu d_{i\nu}, \\ b_i &= (q \cdot p)^2 v_i^2 - (q \cdot v_i)(p \cdot v_i), \\ c_{i,\nu} &= q_\nu(p \cdot v_i) - v_{i\nu}(q \cdot p), \\ d_{i\nu} &= v_{i\nu}(q \cdot v_i) - q_\nu v_i^2, \end{aligned} \quad (\text{A17})$$

where $v_i = k_i - q$, with k_1 and k_2 the four-momenta of the pseudoscalars.

The current can be written as

$$M_\mu = M_{\mu\nu}^{(1)}(\alpha_1\gamma_\nu + \beta_1 p_{1\nu}) + M_{\mu\nu}^{(2)}(\alpha_2\gamma_\nu + \beta_2 p_{2\nu}). \quad (\text{A18})$$

It is convenient to define

$$C_{\pi\pi} = 1, \quad C_{\eta\eta} = \frac{2}{3}, \quad C_{\pi\eta} = \sqrt{\frac{2}{3}}. \quad (\text{A19})$$

Then, for the $\pi^0\pi^0$ final state,

$$\begin{aligned} \alpha_1 &= C_{\pi\pi}[(g_{\rho V} + 2m_p g_{\rho T})D_\rho \Pi_\omega(v_1) \\ &\quad + \frac{1}{3}(g_{\omega V} + 2m_p g_{\omega T})D_\omega \Pi_\rho(v_1)], \\ \beta_1 &= -2C_{\pi\pi}[g_{\rho T} D_\rho \Pi_\omega(v_1) + \frac{1}{3}g_{\omega T} D_\omega \Pi_\rho(v_1)], \\ \alpha_2 &= C_{\pi\pi}[(g_{\rho V} + 2m_p g_{\rho T})D_\rho \Pi_\omega(v_2) \\ &\quad + \frac{1}{3}(g_{\omega V} + 2m_p g_{\omega T})D_\omega \Pi_\rho(v_2)], \\ \beta_2 &= -2C_{\pi\pi}[g_{\rho T} D_\rho \Pi_\omega(v_2) + \frac{1}{3}g_{\omega T} D_\omega \Pi_\rho(v_2)], \end{aligned} \quad (\text{A20})$$

for $\eta^0\eta^0$,

$$\begin{aligned} \alpha_1 &= C_{\eta\eta}[(g_{\rho V} + 2m_p g_{\rho T})D_\rho \Pi_\rho(v_1) \\ &\quad + \frac{1}{3}(g_{\omega V} + 2m_p g_{\omega T})D_\omega \Pi_\omega(v_1)], \end{aligned}$$

$$\begin{aligned} \beta_1 &= -2C_{\eta\eta}[g_{\rho T} D_\rho \Pi_\rho(v_1) + \frac{1}{3}g_{\omega T} D_\omega \Pi_\omega(v_1)], \\ \alpha_2 &= C_{\eta\eta}[(g_{\rho V} + 2m_p g_{\rho T})D_\rho \Pi_\rho(v_2) \\ &\quad + \frac{1}{3}(g_{\omega V} + 2m_p g_{\omega T})D_\omega \Pi_\omega(v_2)], \\ \beta_2 &= -2C_{\eta\eta}[g_{\rho T} D_\rho \Pi_\rho(v_2) + \frac{1}{3}g_{\omega T} D_\omega \Pi_\omega(v_2)], \end{aligned} \quad (\text{A21})$$

and for $\pi^0\eta^0$,

$$\begin{aligned} \alpha_1 &= C_{\pi\eta}[\frac{1}{3}(g_{\rho V} + 2m_p g_{\rho T})D_\rho \Pi_\rho(v_1) \\ &\quad + (g_{\omega V} + 2m_p g_{\omega T})D_\omega \Pi_\omega(v_1)], \\ \beta_1 &= -2C_{\pi\eta}[\frac{1}{3}g_{\rho T} D_\rho \Pi_\rho(v_1) + g_{\omega T} D_\omega \Pi_\omega(v_1)], \\ \alpha_2 &= C_{\pi\eta}[\frac{1}{3}(g_{\rho V} + 2m_p g_{\rho T})D_\rho \Pi_\rho(v_2) \\ &\quad + (g_{\omega V} + 2m_p g_{\omega T})D_\omega \Pi_\rho(v_2)], \\ \beta_2 &= -2C_{\pi\eta}[\frac{1}{3}g_{\rho T} D_\rho \Pi_\omega(v_2) + g_{\omega T} D_\omega \Pi_\rho(v_2)]. \end{aligned} \quad (\text{A22})$$

Because M_μ has the structure

$$M_\mu = A_{\mu\lambda}\gamma_\lambda + B_\mu, \quad (\text{A23})$$

we have, as before, to calculate the trace

$$\begin{aligned} T_B &= \frac{1}{4} \text{Tr} \{(\gamma \cdot p_2 + m_p)(A_{\mu\lambda}\gamma_\lambda + B_\mu)(\gamma \cdot p_1 + m_p) \\ &\quad \times (A_{\mu\lambda}\gamma_\lambda + B_\mu)\}. \end{aligned} \quad (\text{A24})$$

The result is

$$\begin{aligned} T_B &= [m_p^2 - (p_1 \cdot p_2)][\alpha_1\alpha_1^* M_{\mu\nu}^{(1)} M_{\mu\nu}^{(1)} \\ &\quad + (\alpha_1\alpha_2^* + \alpha_2\alpha_1^*)M_{\mu\nu}^{(1)} M_{\mu\nu}^{(2)} + \alpha_2\alpha_2^* M_{\mu\nu}^{(2)} M_{\mu\nu}^{(2)}] \\ &\quad + 2[\alpha_1\alpha_1^* N_1^2 + (\alpha_1\alpha_2^* + \alpha_2\alpha_1^*)(N_1 \cdot N_2) + \alpha_2\alpha_2^* N_2^2] \\ &\quad + 2m_p[(\beta_1\alpha_1^* + \beta_1^*\alpha_1)N_1^2 + (\beta_1\alpha_2^* + \alpha_1^*\beta_2 \\ &\quad + \beta_1^*\alpha_2 + \beta_2^*\alpha_1)(N_1 \cdot N_2) + (\beta_2\alpha_2^* + \beta_2^*\alpha_2)N_2^2] \\ &\quad + [m_p^2 + (p_1 \cdot p_2)][\beta_1\beta_1^* N_1^2 + (\beta_1\beta_2^* + \beta_1^*\beta_2)(N_1 \cdot N_2) \\ &\quad + \beta_2\beta_2^* N_2^2], \end{aligned} \quad (\text{A25})$$

with

$$N_{i\mu} = p_{1\mu}b_i + v_{i\mu}(p_1 \cdot c_i) + p_\mu(p_1 \cdot d_i). \quad (\text{A26})$$

The background cross section is then given by

$$\frac{d\sigma_B}{dt dM d\Omega} = -\zeta^2 \frac{g_0^2}{28\pi^4} \frac{k}{(s - m_p^2)^2} T_B, \quad (\text{A27})$$

and the factor $\zeta = 1$ for different pseudoscalars and $\frac{1}{\sqrt{2}}$ for identical pseudoscalars.

D. Interference cross section

We assume a constant phase ϕ between the continuum background and the resonance signal. The required trace for the interference term is

$$\begin{aligned} T_{\text{int}} &= [m_p^2 - (p_1 \cdot p_2)] [\alpha_1 a_S^* M_{\mu\nu}^{(1)} M_{\mu\nu} + \alpha_2 a_S^* M_{\mu\nu}^{(2)} M_{\mu\nu}] \\ &\quad + 2[\alpha_1 a^*(N^{(1)} \cdot N) + \alpha_2 a_S^*(N^{(2)} \cdot N)] \\ &\quad + 2m_p[(\beta_1 a_S^* + \alpha_1 b_S^*)(N^{(1)} \cdot N) \\ &\quad + (\beta_2 a_S^* + \alpha_2 b_S^*)(N^{(2)} \cdot N)] + [m_p^2 + (p_1 \cdot p_2)] \\ &\quad \times [\beta_1 b_S^*(N^{(1)} \cdot N) + \beta_2 b_S^*(N^{(2)} \cdot N)]. \end{aligned} \quad (\text{A28})$$

The interference cross section is then

$$\frac{d\sigma^{\text{int}}}{dt dM d\Omega} = -\zeta \frac{1}{2^8 \pi^4} \frac{g_0 k}{(s - m_p^2)^2} \times [\cos \phi(T_{\text{int}} + T_{\text{int}}^*) + i \sin \phi(T_{\text{int}} - T_{\text{int}}^*)]. \quad (\text{A29})$$

E. Meson-loop cross section

The loop integral function $I_P(a, b)$ is (see, e.g., Refs. [45, 53] and, for $x < 0$, Ref. [54])

$$I_P(a, b) = \frac{1}{2(a-b)} - \frac{2}{(a-b)^2} \left[f\left(\frac{1}{b}\right) - f\left(\frac{1}{a}\right) \right] + \frac{a}{(a-b)^2} \left[g\left(\frac{1}{b}\right) - g\left(\frac{1}{a}\right) \right], \quad (\text{A30})$$

$$f(x) = \begin{cases} -\left[\arcsin\left(\frac{1}{2\sqrt{x}}\right)\right]^2, & x > \frac{1}{4}, \\ \frac{1}{4} \left[\ln\left(\frac{\eta_{\pm}}{\eta_{-}}\right) - i\pi \right]^2, & 0 < x < \frac{1}{4}, \\ \left[\ln\left(\frac{1}{2\sqrt{-x}} + \sqrt{1 - \frac{1}{4x}}\right) \right]^2, & x < 0, \end{cases} \quad (\text{A31})$$

$$g(x) = \begin{cases} \sqrt{4x-1} \arcsin\left(\frac{1}{2\sqrt{x}}\right), & x > \frac{1}{4}, \\ \frac{1}{2} \sqrt{1-4x} \left[\ln\left(\frac{\eta_{\pm}}{\eta_{-}}\right) - i\pi \right], & 0 < x < \frac{1}{4}, \\ \sqrt{1-4x} \ln\left(\frac{1}{2\sqrt{-x}} + \sqrt{1 - \frac{1}{4x}}\right), & x < 0, \end{cases} \quad (\text{A32})$$

and

$$\eta_{\pm} = \frac{1}{2x} [1 \pm \sqrt{1-4x}]. \quad (\text{A33})$$

For a given two-meson final state ab ,

$$\frac{d\sigma(ab)}{dt dM d\Omega} = -\frac{1}{2^8 \pi^4} \frac{k}{(s - m_p^2)^2} \text{Tr}_{l,ab}, \quad (\text{A34})$$

where the trace $\text{Tr}_{l,ab}$ is given by

$$\begin{aligned} \text{Tr}_{l,ab} = & |A_{l,ab}|^2 [m_p^2 - (p_1 \cdot p_2)] M_{\mu\nu} M_{\mu\nu} \\ & + N_{\mu} N_{\mu} \{ 2|A_{l,ab}|^2 + 2m_p (A_{l,ab} B_{l,ab}^* + A_{l,ab}^* B_{l,ab}) \\ & + [m_p^2 + (p_1 \cdot p_2)] |B_{l,ab}|^2 \}. \end{aligned} \quad (\text{A35})$$

The quantities $A_{l,ab}$ and $B_{l,ab}$ are

$$A_{l,ab} = A_{l,ab}^{\rho} + A_{l,ab}^{\omega}, \quad (\text{A36})$$

$$B_{l,ab} = B_{l,ab}^{\rho} + B_{l,ab}^{\omega}, \quad (\text{A37})$$

$$A_{l,ab}^{\rho(\omega)} = (g_{\rho(\omega)V} + 2m_p g_{\rho(\omega)T}) D_{\rho(\omega)} \sum_P L_{P,\rho(\omega)} t_{PP \rightarrow ab}, \quad (\text{A38})$$

$$B_{l,ab}^{\rho(\omega)} = -2g_{\rho(\omega)T} D_{\rho(\omega)} \sum_P L_{P,\rho(\omega)} t_{PP \rightarrow ab}. \quad (\text{A39})$$

Here D_{ρ} and D_{ω} are the Regge propagators [Eq. (19)], and the sum is over all possible pseudoscalars P in the loop,

$$L_{P,\rho(\omega)} = \frac{e g_{\rho(\omega)PP} I_P(t/m_P^2, M^2/m_P^2)}{2\pi^2 m_P^2}, \quad (\text{A40})$$

where m_P is the mass of the pseudoscalars, $g_{\rho(\omega)PP}$ is the $\rho(\omega)PP$ coupling constant, I_P is the loop integral function (A30) and $t_{PP \rightarrow ab}$ is the t matrix for the transition $PP \rightarrow ab$.

In the calculation of the $a_0(980)$ photoproduction cross section, only the kaon loop contributes. The $\rho(\omega)K^+K^-$ coupling constants can be estimated from that for the $\rho \rightarrow \pi\pi$ decay width with the help of SU(3) symmetry considerations:

$$g_{\rho K^+K^-} = g_{\omega K^+K^-} = \frac{1}{2} g_{\rho\pi\pi} = 2.13. \quad (\text{A41})$$

For the t matrix, we use the parametrization introduced in Ref. [55]:

$$t_{K^+K^- \rightarrow \pi^0\eta}(M) = \frac{g_{a_0\pi\eta} g_{a_0K^+K^-}}{D_{a_0}}, \quad (\text{A42})$$

where

$$D_{a_0}(M) = M_{a_0}^2 - M^2 + \sum_{ab} (\text{Re} \Pi_{ab}(M_{a_0}) - \Pi_{ab}(M)), \quad (\text{A43})$$

$$\begin{aligned} \Pi_{ab}(M) = & \frac{g_{a_0ab}^2}{16\pi^2} \left[-\frac{m_+ m_-}{M^2} \ln \frac{m_a}{m_b} + \rho_{ab}(M) \right. \\ & \left. \times \left(i\pi + \ln \frac{\sqrt{M^2 - m_-^2} - \sqrt{M^2 - m_+^2}}{\sqrt{M^2 - m_-^2} + \sqrt{M^2 - m_+^2}} \right) \right], \end{aligned} \quad (\text{A44})$$

where $m_+ = m_a + m_b$, $m_- = m_a - m_b$. This expression is valid above threshold ($m_a + m_b < M$); below threshold, one should use the analytical continuation. In the case of a_0 , $ab = \pi^0\eta$, K^+K^- , $K^0\bar{K}^0$.

This parametrization was recently employed in the analysis of $\phi \rightarrow \pi^0\eta\gamma$ radiative decays [40]. We use the $a_0(980)$ parameters found in that analysis (“kaon loop” version of the fit):

$$M_{a_0} = 983 \text{ MeV}, \quad g_{a_0\pi\eta} = 2.8 \text{ GeV}, \quad (\text{A45})$$

$$g_{a_0K^+K^-} = g_{a_0K^0\bar{K}^0} = 2.16 \text{ GeV}.$$

The situation with $f_0(980)$ is more complicated, because the $\pi^+\pi^-$ loop also contributes. For the t matrix, we use here the parametrization

$$\begin{aligned} t_{\pi^+\pi^- \rightarrow \pi^0\pi^0} &= \frac{g_{f_0\pi^+\pi^-} g_{\pi^0\pi^0}}{D_{f_0}}, \\ t_{K^+K^- \rightarrow \pi^0\pi^0} &= \frac{g_{f_0\pi^0\pi^0} g_{f_0K^+K^-}}{D_{f_0}}, \end{aligned} \quad (\text{A46})$$

with D_{f_0} given by an expression similar to Eq. (A43) (with $ab = \pi^0\pi^0$, $\pi^+\pi^-$, K^+K^- , $K^0\bar{K}^0$), and $g_{f_0\pi^+\pi^-}^2 = \frac{2}{3} g_{f_0\pi\pi}^2$, $g_{f_0\pi^0\pi^0}^2 = \frac{1}{3} g_{f_0\pi\pi}^2$.

The resonance parameters are taken from the kaon-loop version of the fit [39] obtained in the analysis of $\phi \rightarrow \pi^0\pi^0\gamma$

radiative decay:

$$M_{a_0} = 976.8 \text{ MeV}, \quad g_{f_0\pi^+\pi^-} = -1.43 \text{ GeV},$$

$$g_{f_0K^+K^-} = g_{f_0K^0\bar{K}^0} = 3.76 \text{ GeV}. \quad (\text{A47})$$

In practice, there is strong interference between the $f_0(980)$ resonance and the S -wave isosinglet $\pi\pi$ background, which should be taken into account.

-
- [1] Particle Data Group, J. Phys. G **33**, 1 (2006).
- [2] C. Amsler and F. E. Close, Phys. Lett. **B353**, 385 (1995); Phys. Rev. D **53**, 295 (1996).
- [3] C. J. Morningstar and M. Peardon, Phys. Rev. D **60**, 034509 (1999).
- [4] H. B. Meyer and M. J. Teper, Phys. Lett. **B605**, 344 (2005).
- [5] Y. Chen *et al.*, Phys. Rev. D **73**, 014516 (2006).
- [6] W. Lee and D. Weingarten, Phys. Rev. D **61**, 014015 (1999).
- [7] F. E. Close and A. Kirk, Eur. Phys. J. C **21**, 531 (2001).
- [8] F. Giacosa, T. Gutsche, V. E. Lyubovitskij, and A. Faessler, Phys. Rev. D **72**, 094006 (2005).
- [9] T. Teshima, I. Kitamura, and N. Morisita, J. Phys. G **30**, 663 (2004).
- [10] A. H. Fariborz, Int. J. Mod. Phys. A **19**, 2095 (2004).
- [11] M. Napsuciale and S. Rodriguez, Phys. Rev. D **70**, 094043 (2004).
- [12] A. H. Fariborz, Phys. Rev. D **74**, 054030 (2006).
- [13] F. Giacosa, Phys. Rev. D **75**, 054007 (2007).
- [14] T. Teshima, I. Kitamura, and N. Morisita, Phys. Rev. D **76**, 054002 (2007).
- [15] G. t'Hooft *et al.*, arXiv:0801.2288v1 [hep-ph].
- [16] A. H. Fariborz, R. Jora, and J. Schechter, Phys. Rev. D **77**, 094004 (2008).
- [17] C. McNeile, arXiv:0710.0985v1 [hep-lat]; arXiv:0710.2470v1 [hep-lat].
- [18] E. Klempt and A. Zaitsev, Phys. Rep. **454**, 1 (2007).
- [19] W. Ochs, arXiv:hep-ph/0609207v1.
- [20] P. Minkowski and W. Ochs, Eur. Phys. J. C **9**, 283 (1993).
- [21] D. V. Bugg, Eur. Phys. J. C **52**, 55 (2007).
- [22] M. Albaladejo and J. A. Oller, arXiv:0801.4929v2 [hep-ph].
- [23] S. Narison, Phys. Rev. D **73**, 114024 (2006).
- [24] F. E. Close, A. Donnachie, and Yu. S. Kalashnikova, Phys. Rev. D **65**, 092003 (2002).
- [25] F. E. Close, A. Donnachie, and Yu. S. Kalashnikova, Phys. Rev. D **67**, 074031 (2003).
- [26] M. Guidal, J.-M. Laget, and M. Vanderhaeghen, Nucl. Phys. **A627**, 645 (1997).
- [27] G. Asryan *et al.* (CLAS Collaboration), JLab experiment E-07-009; http://www.jlab.org/exp_prog/generated/apphallb.html (unpublished).
- [28] Yu. S. Kalashnikova, A. Kudryavtsev, A. V. Nefediev, J. Haidenbauer, and C. Hanhart, Phys. Rev. C **73**, 045203 (2006).
- [29] R. Machleidt, K. Holinde, and Ch. Elster, Phys. Rep. **149**, 1 (1987).
- [30] M. G. Olsson and E. T. Osypowski, Phys. Rev. D **17**, 174 (1978).
- [31] S. Nozawa, B. Blankenbecler, and T.-S. H. Lee, Nucl. Phys. **A513**, 459 (1990).
- [32] H. Garcilazo and E. Moya de Guerra, Nucl. Phys. **A562**, 521 (1994).
- [33] R. P. Worden, Nucl. Phys. **B37**, 253 (1972).
- [34] I. S. Barker, A. Donnachie, and J. K. Storrow, Nucl. Phys. **B79**, 431 (1974).
- [35] I. S. Barker and J. K. Storrow, Nucl. Phys. **B137**, 413 (1978).
- [36] H. Morita and T. Suzuki, Prog. Theor. Phys. **86**, 671 (1991).
- [37] G. Grammar and D. Sullivan, in *Electromagnetic Interactions of Hadrons*, Vol. 1, edited by A. Donnachie and G. Shaw (Plenum, New York, 1978).
- [38] G. Asryan *et al.* (CLAS Collaboration), JLab proposal PR-07-009; http://www.jlab.org/exp_prog/proposals/07prop.html (unpublished).
- [39] F. Ambrosino *et al.* (KLOE Collaboration), Eur. Phys. J. C **49**, 473 (2007).
- [40] F. Ambrosino *et al.* (KLOE Collaboration), contributed paper to Lepton Photon 2007, arXiv:0707.4609v1 [hep-ex].
- [41] D. Barberis *et al.* (WA102 Collaboration), Phys. Lett. **B479**, 59 (2000).
- [42] A. Abele *et al.* (Crystal Barrel Collaboration), Eur. Phys. J. C **19**, 667 (2001).
- [43] C. A. Baker *et al.*, Phys. Lett. **B563**, 140 (2003).
- [44] A. Bramon, A. Grau, and G. Pancheri, Phys. Lett. **B283**, 416 (1992).
- [45] N. N. Achasov and V. N. Ivanchenko, Nucl. Phys. **B315**, 465 (1989).
- [46] H. Nagahiro, L. Roca, and E. Oset, arXiv:0802.0455v1 [hep-ph].
- [47] H. Nagahiro, L. Roca, E. Oset, and B. S. Zou, arXiv:0803.4460v1 [hep-ph].
- [48] Yu. S. Kalashnikova, A. E. Kudryavtsev, A. V. Nefediev, C. Hanhart, and J. Haidenbauer, Eur. Phys. J. A **24**, 437 (2005).
- [49] Yu. S. Kalashnikova, A. E. Kudryavtsev, A. V. Nefediev, C. Hanhart, and J. Haidenbauer, Phys. Rev. D **78**, 058501 (2008).
- [50] C.-R. Ji, R. Kaminski, L. Lesniak, A. Szczepaniak, and R. Williams, Phys. Rev. C **58**, 1205 (1998).
- [51] I. Horn *et al.* (CB-ELSA Collaboration), arXiv:0806.4251v1 [nucl-ex].
- [52] M. Fuchs, Ph.D. thesis, Helmholtz-Institut für Strahlen- und Kernphysik, Bonn University (2005); http://hss.ulb.uni-bonn.de/diss_online/math_nat_fak/2005/.
- [53] F. E. Close, N. Isgur, and S. Kumano, Nucl. Phys. **B389**, 513 (1993).
- [54] E. Marco, E. Oset, and H. Toki, Phys. Rev. C **60**, 015202 (1999).
- [55] N. N. Achasov, S. A. Devyanin, and G. N. Shestakov, Yad. Fiz. **32**, 1098 (1980) [Sov. J. Nucl. Phys. **32**, 566 (1980)].